

# Terrestrial planet formation surrounding close binary stars

Elisa V. Quintana<sup>\*</sup>, Jack J. Lissauer

*Space Science and Astrobiology Division 245-3, NASA Ames Research Center, Moffett Field, CA 94035, USA*

Received 18 August 2005; revised 15 June 2006

Available online 22 August 2006

## Abstract

Most stars reside in binary/multiple star systems; however, previous models of planet formation have studied growth of bodies orbiting an isolated single star. Disk material has been observed around both components of some young close binary star systems. Additionally, it has been shown that if planets form at the right places within such disks, they can remain dynamically stable for very long times. Herein, we numerically simulate the late stages of terrestrial planet growth in circumbinary disks around ‘close’ binary star systems with stellar separations  $0.05 \text{ AU} \leq a_B \leq 0.4 \text{ AU}$  and binary eccentricities  $0 \leq e_B \leq 0.8$ . In each simulation, the sum of the masses of the two stars is  $1 M_\odot$ , and giant planets are included. The initial disk of planetary embryos is the same as that used for simulating the late stages of terrestrial planet formation within our Solar System by Chambers [Chambers, J.E., 2001. *Icarus* 152, 205–224], and around each individual component of the  $\alpha$  Centauri AB binary star system by Quintana et al. [Quintana, E.V., Lissauer, J.J., Chambers, J.E., Duncan, M.J., 2002. *Astrophys. J.* 576, 982–996]. Multiple simulations are performed for each binary star system under study, and our results are statistically compared to a set of planet formation simulations in the Sun–Jupiter–Saturn system that begin with essentially the same initial disk of protoplanets. The planetary systems formed around binaries with apastron distances  $Q_B \equiv a_B(1 + e_B) \lesssim 0.2 \text{ AU}$  are very similar to those around single stars, whereas those with larger maximum separations tend to be sparser, with fewer planets, especially interior to 1 AU. We also provide formulae that can be used to scale results of planetary accretion simulations to various systems with different total stellar mass, disk sizes, and planetesimal masses and densities.

© 2006 Elsevier Inc. All rights reserved.

*Keywords:* Planetary formation; Terrestrial planets; Extrasolar planets

## 1. Introduction

More than half of all main sequence stars, and an even larger fraction of pre-main sequence stars, are in binary/multiple star systems (Duquennoy and Mayor, 1991; Mathieu et al., 2000). Virtually all previous models of planet formation, however, have assumed an isolated single star. Of the first 131 extrasolar planet systems that have been confirmed, at least 30 are on so-called S-type orbits that encircle one component of a binary star system, including at least 3 that orbit one member of a triple-star system (Raghavan et al., 2006). The effect of the stellar companion on the formation of these planets, however, remains unclear.

One planet has been detected in a P-type orbit which encircles both members of a binary star system. This planet,

which has a minimum mass of  $\sim 2.5$  times the mass of Jupiter ( $M_J$ ), orbits  $\sim 23 \text{ AU}$  from the center of mass of PSR 1620-26, a radio pulsar binary comprised of a neutron star and a white dwarf in a  $\sim 191$  day stellar orbit (Lyne et al., 1988; Sigurdsson and Phinney, 1993; Sigurdsson et al., 2003). The most plausible model for its formation is accretion within a metal-rich disk produced by post-main sequence Roche lobe overflow (Lissauer, 2004). Planets have not been detected in a P-type orbit around two main sequence stars, but short-period binaries are not included in precise Doppler radial velocity search programs because of their complex and varying spectra. Planets in P-type orbits around the eclipsing binary star system CM Draconis have been searched for using the eclipse timing variation method (Deeg et al., 2000), but results were not definitive. Two substellar companions have been detected around the G6V star HD 202206, with minimum masses of  $17.4 M_J$  (at 0.83 AU) and  $2.44 M_J$  (at 2.55 AU) (Udry et al., 2002). The inner companion is so massive that it is considered to be a brown dwarf, and it is likely that the outer companion formed

<sup>\*</sup> Corresponding author.

E-mail address: [equintan@pollack.arc.nasa.gov](mailto:equintan@pollack.arc.nasa.gov) (E.V. Quintana).

from within a circumbinary (star-brown dwarf) disk (Correia et al., 2005). A more general discussion of the detectability of circumbinary planets is presented by Muterspaugh (2005). Note also that the observation of two small moons orbiting in nearly circular/planar orbits about Pluto–Charon (Weaver et al., 2006), a system which is like a binary with an 8/1 mass ratio, suggests that accretion can occur in P-type orbits about close binaries.

The main objective of this article is to numerically examine the late stages of terrestrial planet formation around both members of a binary star system. The existence of Earth-like planets in orbit about one or both components of main sequence binary stars has yet to be determined, though ground- and space-based efforts to search for extrasolar terrestrial planets are currently in development. An additional benefit of understanding the differences between planet formation around single stars and that around close binaries is that for eclipsing binaries, the contrast ratio between brightness of the stars and that of the planet(s) is reduced during the eclipse. For a total eclipse of identical stars, this reduction is a factor of two; as lower mass main sequence stars can be just slightly smaller but significantly less luminous, the detectability of the planet can be enhanced by more than a factor of two when the fainter star transits the brighter one. In an evolved close binary having undergone mass transfer, the fainter star can actually completely eclipse its much brighter companion, leading to an even larger improvement in planetary detectability.

In the conventional model of planet formation, terrestrial planets are believed to have formed by an accretion process from within a disk of gas and dust that has remained around a newly formed star (Safronov, 1969; Lissauer, 1993). The co-existence of disks of material with stars that possess a stellar companion support the idea that planet formation within binary star systems may be common. Circumbinary disk material has been detected through millimeter and mid-infrared excess emission around several spectroscopic pre-main sequence binary star systems with stellar semimajor axes  $a_B \lesssim 1$  AU. These systems include GW Ori (Mathieu et al., 1995), UZ Tau E (Jensen et al., 1996), and DQ Tau (Mathieu et al., 1997). The masses of these disks are each comparable to or exceed the minimum mass of the solar nebula,  $\sim 0.01$  solar mass ( $M_\odot$ ) (Weidenschilling, 1977), and are also comparable to the masses of disks found around single stars.

Numerical models of circumbinary disks find that, for binary star systems with binary eccentricities ( $e_B$ ) increasing from 0 to 0.25, the inner edge of a gaseous disk is truncated to within  $\sim 1.8$ – $2.6$  times the semimajor axis of the binary stars' mutual orbit ( $a_B$ ) (Artymowicz and Lubow, 1994; Lubow and Artymowicz, 2000). A star with a giant planet orbiting interior to the terrestrial planet region is dynamically a binary system of extreme mass ratio. Raymond et al. (2005) showed that planetary embryos can accrete into terrestrial planets around a star that has a close-in (between 0.15 and 0.5 AU) Jupiter-mass planet.

Herein, we simulate terrestrial planetary accretion within a circumbinary disk of protoplanets around ‘close’ ( $a_B = 0.05$ – $0.4$  AU) binary star systems that each have a combined stellar mass of  $1 M_\odot$ . Our numerical method and the initial

states of the systems that we have simulated are given in Section 2. Section 3 examines the regions of stability for test particles orbiting about these binary star systems. The results of the close binary accretion simulations, including a quantitative analysis of the final planetary systems formed, are presented in Section 4. Our conclusions are discussed in Section 5. Appendix A presents new simulations of the late stages of terrestrial planet formation in the Sun–Jupiter–Saturn system that we have performed to facilitate comparisons between planet growth around single and close binary stars, and simulations using an initial disk of bodies whose eccentricities are forced by the binary stars are presented in Appendix B. In Appendix C, we discuss the scaling of our results to systems with different planetesimal densities, disk sizes, and stellar masses.

## 2. Initial conditions and numerical model

The combined mass of the binary stars is equal to  $1 M_\odot$  in all of the simulations, with the stellar mass ratio  $\mu$  (the ratio of the secondary star’s mass to the total stellar mass) equal to either 0.2 or 0.5. Binary star separations in the range  $a_B = 0.05$ – $0.4$  AU are examined, while  $e_B$  begins at 0,  $1/3$ , 0.5, or 0.8 such that the stellar apastron  $Q_B \equiv a_B(1 + e_B)$  is  $0.05 \text{ AU} \leq Q_B \leq 0.4 \text{ AU}$ . Not all combinations of these stellar parameters, however, are used. For most of the simulations, the midplane of the circumbinary disk begins coplanar to the stellar orbit, but for one set of binary star parameters a relative inclination of  $i = 30^\circ$  is investigated. Although a stellar companion present during the earlier stages of planet formation would likely force the planetesimal disk into the plane of the binary orbit, many binary stars may originate as unstable triple star systems which could produce a binary star system with an accretion disk at a high relative inclination. It is also possible that a companion may have been captured around a single star that possesses an accretion disk.

Giant planets are included in the simulations, as they are in most simulations of the late stages of terrestrial planet accumulation in our Solar System (Chambers, 2001; Appendix A). In all of the planetary accretion simulations presented herein, a Jupiter-mass planet is placed in the system at  $a_J = 5.2$  AU, with an eccentricity of  $e_J = 0.048$  and an inclination of  $i_J = 0.36^\circ$  relative to the midplane of the disk. Apart from a single set of runs in which the stars are separated by  $a_B = 0.05$  AU and travel on an initially circular orbit coplanar with the midplane of the disk, a second giant planet of Saturn’s mass, with  $a_S = 9.54$  AU,  $e_S = 0.053$ , and  $i_S = 0.89^\circ$  relative to the midplane of the disk, is also included. The effect of the stellar perturbations on these giant planets is discussed in Section 4.2.

### 2.1. Circumbinary disk model

The initial conditions for the bodies in the circumbinary disk are based upon earlier numerical simulations of the late stages of terrestrial planet formation in the Sun–Jupiter–Saturn (SJS) system (Chambers, 2001) which resulted in the formation of planetary systems with masses and orbits similar to the terrestrial planets in the Solar System (see Appendix A). In this

model, 14 planetary embryos (each with a mass of 0.0933 times the mass of the Earth,  $M_{\oplus}$ ) are embedded in a disk of 140 smaller planetesimals (each with a mass of 0.00933  $M_{\oplus}$ ), all lying between 0.36 and 2.05 AU of the center of mass of the binary stars. The radii of these bodies are calculated assuming a material density of  $3 \text{ g cm}^{-3}$ . All other initial orbital elements were chosen at random, with the eccentricities ranging from 0–0.01, and inclinations relative to the mean plane of the disk  $\leq 0.5^\circ$ . Analyses of trajectories around close binaries show that closed, near circular, non-crossing orbits occur in situations such as this (Pichardo et al., 2005; see especially their Figs. 6 and 9). In Appendix B, we present one set of simulations that was run using a disk of planetesimals and embryos with initial eccentricities determined by perturbations from the binary.

In the majority of our simulations, the initial planetesimal/embryo disk extends closer to the stars than the region in which planetesimals are expected to be able to form within a *gas-free* disk (Moriwaki and Nakagawa, 2004). However, calculations show that planetesimal growth occurs over a much greater region within *gas-rich* circumstellar (S-type orbits) disks than within analogous regions of gas-free disks (Kortenkamp and Wetherill, 2000; cf. Thebault et al., 2006), and we would expect an analogous situation for P-type orbital regions. Moreover, it is also possible that at least the initial phases of planetesimal growth can occur farther from the stars, and the planetesimals can then migrate inwards as a consequence of gas drag.

## 2.2. Numerical method

To examine both the orbital stability and accretion of bodies in a disk, we use one of the two symplectic  $N$ -body algorithms that we developed to examine planetary accretion in binary star systems (Chambers et al., 2002). The ‘close binary’ algorithm (used in the simulations presented in this article) was designed to examine accretion in P-type orbits around binary stars. The ‘wide binary’ algorithm, which follows bodies in S-type orbits within binary star systems, was recently used to simulate the late stages of terrestrial planet formation around each star of the nearest binary star system to the Sun,  $\alpha$  Centauri AB (Quintana et al., 2002, 2003). In these simulations, which began with an initial disk mass distribution virtually identical to the disk discussed above, from 3 to 5 terrestrial planets formed on stable orbits around each individual component in  $\alpha$  Cen AB provided the initial inclination of the disk relative to the stellar orbit began at or below  $\sim 30^\circ$ . Numerous simulations of terrestrial planet formation in S-type orbits in main sequence binary star systems, with the aim of examining a larger binary star parameter space, will be presented in Quintana et al. (2007, in preparation).

The close binary algorithm calculates the temporal evolution of the position and velocity of each body in the disk with respect to the center of mass of the binary stars, subject to gravitational perturbations from both stars and to gravitational interactions and completely inelastic collisions among the bodies. Bodies are removed if their orbit extends more than 100 AU from the more massive star, or if they orbit too close to the center of

mass of the binary stars. For selected simulations with larger stellar separations, material is removed if its distance from the center of mass exceeds the smaller star’s apastron distance by less than 0.1 AU. A time-step of 7 days is used for the bodies in the disk, while the binary stars are given a time-step that is shorter by approximately the ratio of the binary period to the orbital period of the innermost planetesimal (see Chambers et al., 2002 for details). The period of the innermost body is 55.09 days, so the choice of a 7-day time-step may not accurately follow the evolution of the innermost bodies, which could lead to errors, especially concerning the amount of mass lost inside. We are comparing our results, however, to the simulations in the Sun–Jupiter–Saturn system (Chambers, 2001) and to simulations around each star in  $\alpha$  Cen AB, each of which used a 7-day time-step, so the differences that we find should be real.<sup>1</sup>

Because these  $N$ -body systems are chaotic, each binary star system under study is simulated five or six times with slightly different initial conditions for the circumbinary disk. Of the 154 rocky embryos and smaller planetesimals, one planetesimal near 1 AU is initially displaced by 1, 2, 3, 4, or 5 m along its orbit with all other parameters within a given set remaining the same. The simulations are labeled as follows: CB- $a_B$ - $e_B$ - $\mu$ - $x$ , where  $a_B$  is the binary semimajor axis,  $e_B$  is the binary eccentricity,  $\mu$  is the stellar mass ratio, and  $x$  (= a, b, c, d, e, or f) signifies each realization of a given system. If the mid-plane of the initial planetesimal disk is inclined relative to that of the binary star orbital plane, the inclination angle is listed between  $\mu$  and  $x$ , but when they are coplanar (as for most of our simulations), no value is given. The first run in each set (the ‘a’ integrations) begins with the ‘standard’ bi-modal circumbinary disk mass distribution. In the remaining runs within a set, a planetesimal near 1 AU is initially displaced by 1 m along its orbit (for the ‘b’ integrations), by 2 m along its orbit (for

<sup>1</sup> To investigate the statistical validity of simulations performed using a 7-day time-step, we performed test particle simulations for five of the binary star systems that are examined in this article using time-steps of 3.5, 3.6, and 7 days for each system. For the binary star systems with stellar parameters ( $a_B$ ,  $e_B$ ,  $\mu$ ) equal to (0.05, 0, 0.5) and (0.1, 0.8, 0.5), from 25 to 50 test particles were placed around each system at 0.01 AU intervals, beginning at the distance from the center of mass of the stars at which bodies are removed. For the binary star systems with ( $a_B$ ,  $e_B$ ,  $\mu$ ) equal to (0.2, 0.5, 0.5), (0.3, 1/3, 0.5), and (0.4, 0, 0.5), the smallest semimajor axis for which bodies can be stable was determined,  $a_c$  (described further in Section 3), and test particles were placed between ( $a_c - 0.25$  AU) and ( $a_c + 0.25$  AU), with 0.01 AU intervals. All other orbital elements were chosen at random, with eccentricities  $e \leq 0.01$  and inclinations  $i \leq 0.01$  radian, but were kept the same for each set of simulations. The giant planets were not included and the test particle orbits were followed for 10 Myr. For the binary system with  $a_B = 0.05$  AU that began on an initially circular orbit, the orbital elements of the surviving test particles were nearly identical. Particles in other systems, especially close to the stability limit, showed larger variations. The differences in results between the runs with 3.5-day time-steps and 3.6-day time-steps, however, were almost as large as the differences from the 7-day time-step runs, indicating that the dominant source of variation was chaos rather than systematic inaccuracy of the integrations. Moreover, in many of our simulations the innermost planetesimal survived the entire integration intact, with little variation in its principal orbital elements (as was the case for some of our simulations of planetary growth; see, for example, Fig. 1). We therefore conclude that the use of a 7-day time-step does not significantly degrade the statistical validity of our integrations.

the “c” integrations), etc. The evolution of the material in the disk is initially followed for 200 Myr. If it appeared that further collisions among the planets were fairly likely, individual integrations were continued for total simulation times of 500 Myr (or 550 Myr in one case) or 1 Gyr. In simulations that resulted in the formation of just one planet, the integrations were stopped after the last collision or ejection. The results of each accretion simulation are presented in Table 2 and discussed in Section 4.

### 3. Orbital stability around close binary star systems

The dynamical stability of test particles in P-type orbits has been previously examined for binary star systems with  $\mu$  ranging from 0.1 to 0.5 and binary eccentricities  $e_B$  between 0.0 and 0.7 (Holman and Wiegert, 1999). In that study, test particles were placed in the binary orbital plane between  $1.0a_B$  and  $5.0a_B$  (with  $0.1a_B$  increments) at eight equally spaced longitudes per semimajor axis, and the system was evolved forward in time for  $10^4$  binary periods. The closest distance to the binary at which all eight particles survived (the ‘critical semimajor axis,’  $a_c$ ) was calculated for each system. Depending on  $e_B$  and  $\mu$ ,  $a_c$  was found to lie within  $2.0a_B$ – $4.1a_B$ . Many of these simulations also revealed an unstable region beyond  $a_c$  that corresponded to one of the system’s  $n:1$  mean motion resonances, followed by an additional outer region of stability.

We performed a similar analysis for the close binary configurations examined herein, with the integration time extending to  $10^6$  binary orbital periods. Test particles were placed between  $1.8a_B$  and  $5.0a_B$  (with  $0.1a_B$  increments) at eight equally spaced longitudes. Integrations were performed using the close binary algorithm. Particles were removed from the simulation if they fell within  $0.01a_B$  from the more massive star or if their distance exceeded  $100a_B$ . For each system, Table 1 gives the smallest semimajor axis at which bodies at all 8 longitudes survive the integration,  $a_c$ . In the close binary systems with  $e_B = 1/3$ , regions of instability were found beyond  $a_c$ , and the minimum semimajor axis at and beyond which all test particles survive is listed in brackets in Table 1. Analogous integrations were performed with finer increments of  $0.01a_B$  to find the innermost semimajor axis for which at least one body survived, given by  $a_c^*$  in Table 1. These results are consistent with those of Holman and Wiegert (1999), who found a (roughly) linear dependence of the critical semimajor axis on  $e_B$ . Note that for a given  $e_B \geq 1/3$ , the region cleared of test particles is greater

for  $\mu = 0.2$  than it is for  $\mu = 0.5$ , presumably because the apastron distance of the smaller star from the center of mass of the system is larger for  $\mu = 0.2$ . For each close binary accretion simulation, the ratio of the semimajor axis of the innermost final planet ( $a_p$ ) to the innermost stable orbit of the system ( $a_c^*$ ) is presented in Table 2.

### 4. Planetary accretion simulations

Fig. 1 displays the accretion evolution of system CB\_05\_0\_0.5<sup>†</sup>\_a (the dagger signifies that only one gas giant, a Jupiter-mass planet at 5.2 AU, is included). The eccentricity of each body is shown as a function of semimajor axis, and the radius of each symbol is proportional to the radius of the body that it represents. Throughout the simulation, the larger embryos remain on orbits with  $e \lesssim 0.1$ , whereas the planetesimals become more dynamically excited with time during the first  $\sim 10$ – $20$  Myr. Between  $\sim 5$  and 50 Myr, a trend occurs in which planetesimal eccentricities increase with increasing semimajor axis as a consequence of perturbations by Jupiter. All but one of the planetesimals are either swept up by the larger embryos or are ejected from the system. The first planetesimal ejection occurs at  $\sim 12$  Myr, while the only lost embryo was ejected at  $\sim 37$  Myr. No bodies in this system traveled closer to the binary orbit than the initial semimajor axis of the innermost planetesimal; indeed, the innermost planetesimal was the one that survived without impact. After 500 Myr elapsed, 6 planets with masses between  $0.11$  and  $0.61 M_\oplus$  orbited within 2.3 AU; these planets incorporated 84% of the initial disk mass. Despite the apparent crowding, the system appears to be quite stable; no bodies are lost or accreted between 92.7 Myr and the end of the simulation.

Fig. 2 (CB\_05\_0\_0.5<sup>†</sup>\_d) shows the growth of planets formed around a binary star system identical to that shown in Fig. 1, but in this case the initial disk mass is slightly different (one planetesimal near 1 AU is shifted by 3 m along its orbit). Note that the evolution of the disk in this figure (and subsequent figures) is shown beginning at  $t = 0.2$  Myr, as the plotted properties of the disk at  $t = 0$  are identical to those shown in the first panel in Fig. 1. The stellar and giant planet perturbations have a similar effect on the disk as in the simulation shown in Fig. 1. In this case, three terrestrial-mass planets have formed within 1.5 AU, while one planetesimal remains at 2.2 AU, all together incorporating 81% of the initial mass in the disk. The differences in the final planets formed from two simulations with almost identical initial conditions (Fig. 1 vs Fig. 2) demonstrate the chaotic nature of these  $N$ -body systems.

Fig. 3 shows run CB\_05\_0\_0.5\_c, which included a Saturn-like giant planet in addition to the Jupiter-like one. Nonetheless, the outcome looks intermediate between the systems shown in Figs. 1 and 2. A comparison between all of the CB\_05\_0\_0.5<sup>†</sup> runs with the CB\_05\_0\_0.5 runs (Table 2 and Fig. 7) suggests that the extra perturbations of “Saturn” may reduce the expected number of terrestrial planets formed, but the effects are small enough that there is considerable overlap among the chaos-broadened distributions of outcomes. Note that these distributions also overlap the results of simulations of terrestrial

Table 1  
Stability regions for test particles orbiting close binary stars

$e_B$	$\mu$	$a_c$ ( $a_B$ )	$a_c^*$ ( $a_B$ )
0	0.2	2.2	1.80
0	0.5	2.3	2.01
1/3	0.2	3.5 [3.8]	3.15
1/3	0.5	3.2 [3.5]	2.99
0.5	0.2	3.9	3.40
0.5	0.5	3.6	2.98
0.8	0.2	4.3	3.86
0.8	0.5	3.9	3.19

Table 2  
Statistics for final planetary systems

Run	$t$ (Myr)	$N_p$	$N_m$	$a_p/a_c^*$	$q_p/Q_B$	$S_m$	$S_s$	$S_d$	$S_c$	$S_r$	$m_1$ (%)	$E/E_0$	$L/L_0$	$L_Z/L_{Z_0}$
CB_05_0 <sup>+</sup> _5_a <sup>a</sup>	500	6	1	3.53	7.12	0.288	27.1	0.0041	32.3	0.226	15.71	1.13	0.94	0.93
CB_05_0 <sup>+</sup> _5_b <sup>a</sup>	200	4	1	3.48	7.18	0.388	36.3	0.0063	29.5	0.343	13.57	1.14	0.93	0.93
CB_05_0 <sup>+</sup> _5_c <sup>a</sup>	500	4	1	3.48	7.28	0.515	34.4	0.0008	36.8	0.289	14.29	1.13	0.93	0.93
CB_05_0 <sup>+</sup> _5_d <sup>a</sup>	200	3	1	5.00	10.47	0.458	43.0	0.0047	34.7	0.410	18.93	1.18	0.91	0.91
CB_05_0 <sup>+</sup> _5_e <sup>a</sup>	200	2	1	7.47	16.02	0.905	40.0	0.0110	213.8	0.437	28.93	1.33	0.82	0.81
$\bar{x}$	320	3.8	1	4.59	9.61	0.511	36.2	0.0054	69.4	0.341	18.29	1.18	0.91	0.90
$D$	...	0.28	0.58	...	...	0.22	0.28	0.48	0.35	0.28	0.70	0.67	0.67	0.70
$P$	...	0.832	0.066	...	...	0.968	0.832	0.200	0.572	0.810	0.014	0.021	0.021	0.014
CB_05_0_5_a	500	3	1	3.42	7.52	0.500	45.3	0.0069	30.8	0.379	15.71	1.15	0.93	0.93
CB_05_0_5_b	200	3	1	3.46	7.29	0.561	48.4	0.0252	29.5	0.454	24.29	1.23	0.88	0.88
CB_05_0_5_c	500	5	1	5.00	10.95	0.355	30.3	0.0026	31.4	0.309	11.43	1.11	0.95	0.94
CB_05_0_5_d	200	3	1	5.12	10.50	0.473	42.4	0.0049	29.7	0.364	12.50	1.13	0.94	0.94
CB_05_0_5_e	500	5	1	3.43	7.17	0.294	27.8	0.0066	27.7	0.204	11.43	1.10	0.96	0.95
$\bar{x}$	380	3.8	1	4.09	8.68	0.437	38.84	0.0092	29.8	0.342	15.07	1.14	0.93	0.93
$D$	...	0.37	0.58	...	...	0.34	0.37	0.41	0.67	0.38	0.80	0.80	0.77	0.77
$P$	...	0.501	0.066	...	...	0.620	0.501	0.355	0.021	0.457	0.003	0.003	0.005	0.005
CB_075_1/3_5_a	200	3	1	1.56	3.66	0.436	40.2	0.0166	27.7	0.363	24.64	1.02	1.00	0.98
CB_075_1/3_5_b	200	2	0	5.89	16.47	0.910	54.1	0.0310	167.7	0.290	52.50	0.75	1.06	1.06
CB_075_1/3_5_c	200	3	0	2.21	5.96	0.566	41.3	0.0047	37.5	0.306	13.57	1.08	0.95	0.95
CB_075_1/3_5_d	200	2	3	5.50	13.39	0.487	42.9	0.0282	96.2	0.285	59.64	0.68	1.13	1.13
CB_075_1/3_5_e	200	3	1	1.54	3.58	0.489	42.9	0.0092	35.3	0.255	21.79	1.15	0.92	0.92
$\bar{x}$	200	2.6	1	3.34	8.61	0.578	44.28	0.0179	72.9	0.300	34.43	0.94	1.01	1.01
$D$	...	0.48	0.34	...	...	0.42	0.55	0.37	0.37	0.64	0.37	0.80	0.935	0.968
$P$	...	0.200	0.620	...	...	0.337	0.096	0.479	0.501	0.032	0.501	0.003	0.000	0.000
CB_1_0_5_a	200	4	1	2.40	5.70	0.478	36.1	0.0033	32.7	0.305	17.14	1.11	0.94	0.94
CB_1_0_5_b	200	5	1	1.80	3.74	0.313	29.8	0.0017	29.7	0.314	11.06	1.07	0.97	0.97
CB_1_0_5_c	200	4	1	1.88	4.22	0.335	33.2	0.0040	32.9	0.253	11.43	1.06	0.97	0.97
CB_1_0_5_d	200	4	1	2.97	6.44	0.297	30.7	0.0044	35.9	0.263	17.14	1.06	0.96	0.96
CB_1_0_5_e	200	4	1	2.62	5.84	0.345	30.1	0.0036	39.0	0.314	21.43	1.19	0.90	0.90
$\bar{x}$	200	4.2	1	2.33	5.19	0.354	32.0	0.0034	34.0	0.290	15.64	1.10	0.95	0.95
$D$	...	0.68	0.58	...	...	0.74	0.74	0.70	0.47	0.57	0.77	0.80	0.77	0.77
$P$	...	0.019	0.066	...	...	0.008	0.008	0.014	0.212	0.071	0.005	0.003	0.005	0.005
CB_1_0_2_a	200	3	1	2.00	3.85	0.440	41.1	0.0038	35.6	0.314	19.29	1.11	0.94	0.94
CB_1_0_2_b	200	4	1	2.63	5.45	0.322	34.9	0.0053	29.7	0.422	16.79	1.14	0.94	0.94
CB_1_0_2_c	200	4	0	3.04	5.86	0.451	33.6	0.0019	33.4	0.317	11.79	1.07	0.96	0.96
CB_1_0_2_d	500	4	1	1.95	3.73	0.500	29.7	0.0041	36.9	0.393	20.00	1.17	0.91	0.91
CB_1_0_2_e	500	5	0	2.56	5.00	0.414	32.5	0.0031	31.2	0.305	18.93	1.13	0.94	0.94
$\bar{x}$	320	4.0	0.6	2.44	4.78	0.425	34.36	0.0036	33.4	0.350	17.36	1.12	0.94	0.94
$D$	...	0.48	0.34	...	...	0.38	0.54	0.67	0.45	0.37	0.67	0.80	0.87	0.90
$P$	...	0.200	0.620	...	...	0.457	0.103	0.021	0.269	0.479	0.021	0.003	0.001	0.001
CB_1_8_5_a	200	3	2	2.29	4.31	0.440	35.3	0.0284	61.2	0.273	31.79	0.90	1.01	0.99
CB_1_8_5_b	500	2	0	2.45	4.74	0.667	45.3	0.0100	78.8	0.305	38.93	0.95	0.98	0.98
CB_1_8_5_c	200	3	2	1.84	3.33	0.634	43.4	0.0101	55.9	0.219	31.79	1.00	0.97	0.96
CB_1_8_5_d	200	3	2	1.90	3.82	0.574	49.0	0.0276	37.2	0.274	39.64	1.06	0.95	0.93
CB_1_8_5_e	200	4	1	1.52	2.88	0.328	36.5	0.0451	33.9	0.291	30.36	1.09	0.95	0.91
$\bar{x}$	650	3.0	1.4	2.00	3.82	0.529	41.9	0.0242	53.4	0.272	34.50	1.00	0.97	0.96
$D$	...	0.45	0.41	...	...	0.37	0.26	0.52	0.50	0.67	0.77	0.80	0.97	0.87
$P$	...	0.269	0.374	...	...	0.479	0.889	0.135	0.155	0.021	0.005	0.003	0.000	0.001
CB_1_8_2_a	500	2	0	1.98	4.86	0.544	83.5	0.0841	19.7	0.527	46.79	0.95	1.03	0.97
CB_1_8_2_b	500	3	0	1.93	4.50	0.468	38.7	0.0276	57.5	0.347	32.86	1.09	0.92	0.90
CB_1_8_2_c	200	3	1	2.13	4.91	0.433	43.5	0.0060	39.5	0.208	35.71	0.93	1.02	1.02
CB_1_8_2_d	165	1	0	2.82	6.78	1.000	...	0.0109	$\infty$	0.376	46.43	0.95	0.95	0.95
CB_1_8_2_e	200	3	1	1.52	3.96	0.490	47.6	0.0378	30.5	0.368	30.00	1.02	0.98	0.95
$\bar{x}$	313	2.4	0.4	2.07	5.00	0.587	59.4	0.0333	40.9	0.365	38.36	0.99	0.98	0.96
$D$	...	0.48	0.50	...	...	0.39	0.52	0.47	0.30	0.38	0.71	0.80	0.94	0.77
$P$	...	0.200	0.155	...	...	0.435	0.135	0.212	0.742	0.457	0.012	0.003	0.000	0.005
CB_1_0_5_30 <sup>o</sup> _a	500	4	0	2.47	5.46	0.453	38.5	0.1182	29.8	0.387	28.21	1.42	0.83	0.74
CB_1_0_5_30 <sup>o</sup> _b	500	2	1	2.18	5.06	0.724	50.5	0.0938	60.1	0.513	22.50	1.53	0.78	0.71

(continued on next page)

Table 2 (continued)

Run	$t$ (Myr)	$N_p$	$N_m$	$a_p/a_c^*$	$q_p/Q_B$	$S_m$	$S_s$	$S_d$	$S_c$	$S_r$	$m_1$ (%)	$E/E_0$	$L/L_0$	$L_Z/L_{Z_0}$
CB_1_0_5_30°_c	500	3	0	1.98	4.29	0.515	48.1	0.1473	25.5	0.467	18.93	1.48	0.82	0.71
CB_1_0_5_30°_d	200	4	1	1.79	3.69	0.421	36.5	0.0157	26.7	0.293	18.57	1.12	0.95	0.94
CB_1_0_5_30°_e	550	2	0	4.07	9.50	0.913	49.9	0.1610	186.1	0.361	42.14	1.21	0.85	0.72
$\bar{x}$	450	3.0	0.4	2.50	5.60	0.605	44.7	0.1072	65.6	0.404	26.07	1.35	0.85	0.76
$D$	...	0.31	0.50	...	...	0.39	0.32	0.77	0.47	0.19	0.30	0.54	0.57	0.77
$P$	...	0.718	0.155	...	...	0.435	0.669	0.005	0.212	0.994	0.742	0.110	0.071	0.005
CB_15_1/3_5_a	200	2	0	2.03	5.16	0.736	52.4	0.0203	79.5	0.174	56.79	0.77	1.09	1.08
CB_15_1/3_5_b	200	3	3	1.63	3.91	0.600	33.6	0.0070	83.7	0.313	44.64	1.09	0.92	0.91
CB_15_1/3_5_c	200	2	0	2.40	6.19	0.714	39.5	0.0135	120.6	0.275	45.00	0.86	1.02	1.01
CB_15_1/3_5_d	200	3	1	1.74	4.10	0.626	44.3	0.0134	60.4	0.270	37.86	0.93	1.00	0.99
CB_15_1/3_5_e	200	3	2	1.27	3.10	0.497	39.9	0.0066	57.7	0.260	39.64	1.00	0.97	0.96
$\bar{x}$	200	2.6	1.2	1.82	4.49	0.635	41.9	0.0122	80.4	0.258	44.79	0.93	1.00	0.99
$D$	...	0.48	0.34	...	...	0.61	0.32	0.39	0.90	0.74	0.97	0.80	0.94	0.97
$P$	...	0.200	0.620	...	...	0.049	0.693	0.435	0.001	0.008	0.000	0.003	0.000	0.000
CB_2_0_5_a	200	3	1	1.11	2.35	0.545	47.6	0.0064	40.0	0.182	23.93	1.02	0.97	0.97
CB_2_0_5_b	200	5	1	1.15	2.56	0.429	29.6	0.0058	45.8	0.248	20.00	1.08	0.94	0.94
CB_2_0_5_c	200	4	2	1.17	2.42	0.519	32.7	0.0075	58.4	0.405	32.50	1.12	0.91	0.91
CB_2_0_5_d	500	4	1	1.07	2.21	0.553	38.8	0.0053	34.2	0.298	32.14	1.12	0.94	0.93
CB_2_0_5_e	200	2	1	2.35	4.85	0.633	36.1	0.0052	109.4	0.242	43.57	0.95	0.98	0.97
$\bar{x}$	260	3.6	1.2	1.37	2.88	0.536	37.0	0.0060	57.6	0.275	30.43	1.06	0.95	0.94
$D$	...	0.28	0.58	...	...	0.41	0.34	0.45	0.41	0.64	0.44	0.80	0.87	0.87
$P$	...	0.832	0.066	...	...	0.35	0.620	0.269	0.35	0.032	0.285	0.003	0.001	0.001
CB_2_0_2_a	200	3	2	1.24	2.30	0.659	59.0	0.0067	41.5	0.263	41.43	0.92	1.02	1.02
CB_2_0_2_b	200	3	0	1.29	2.35	0.632	41.8	0.0041	84.2	0.253	48.57	1.08	0.93	0.92
CB_2_0_2_c	500	3	3	1.28	2.51	0.661	48.1	0.0096	62.1	0.233	41.07	1.07	0.93	0.93
CB_2_0_2_d	200	3	0	2.40	4.99	0.461	35.9	0.0073	60.4	0.220	45.00	0.85	1.05	1.05
CB_2_0_2_e	200	3	0	1.27	2.43	0.487	49.0	0.0058	41.0	0.323	30.36	1.02	0.98	0.97
$\bar{x}$	260	3.0	1	1.50	2.92	0.580	46.8	0.0067	57.8	0.258	41.29	0.99	0.98	0.98
$D$	...	0.41	0.50	...	...	0.42	0.38	0.38	0.68	0.74	0.77	0.80	0.97	0.97
$P$	...	0.355	0.155	...	...	0.337	0.457	0.457	0.019	0.008	0.005	0.003	0.000	0.000
CB_2_5_5_a	146	1	0	2.35	5.44	1.000	...	0.0193	$\infty$	0.147	73.58	0.74	1.07	1.07
CB_2_5_5_b	200	2	0	2.25	4.65	0.890	57.2	0.0021	152.4	0.169	67.50	0.73	1.11	1.11
CB_2_5_5_c	154	1	0	3.56	8.54	1.000	...	0.0328	$\infty$	0.378	85.71	0.49	1.31	1.30
CB_2_5_5_d	115	1	0	2.70	5.92	1.000	...	0.0190	$\infty$	0.263	79.29	0.64	1.16	1.15
CB_2_5_5_e	200	2	0	1.78	5.20	0.590	32.4	0.0104	185.7	0.155	62.50	0.67	1.15	1.15
$\bar{x}$	163	1.4	0.0	2.53	5.95	0.896	52.2	0.0167	179.0	0.222	73.72	0.65	1.16	1.15
$D$	...	0.74	0.67	...	...	0.77	0.70	0.41	0.97	0.74	0.97	0.80	0.97	0.97
$P$	...	0.008	0.021	...	...	0.005	0.014	0.374	0.000	0.008	0.000	0.003	0.000	0.000
CB_2_5_2_a	200	2	1	1.15	2.95	0.547	36.9	0.0081	133.3	0.127	69.29	0.66	1.17	1.16
CB_2_5_2_b	200	2	0	1.85	4.45	0.563	30.9	0.0126	203.1	0.179	63.21	0.69	1.13	1.12
CB_2_5_2_c	500	2	1	1.82	4.62	0.691	67.6	0.0080	71.0	0.425	80.36	0.72	1.13	1.12
CB_2_5_2_d	500	2	0	1.39	3.21	0.828	54.2	0.0244	141.1	0.083	77.15	0.73	1.09	1.09
CB_2_5_2_e	200	2	1	1.36	3.34	0.860	46.5	0.0099	190.0	0.184	66.79	0.75	1.09	1.09
$\bar{x}$	320	2.0	0.6	1.51	3.71	0.698	47.2	0.0126	147.7	0.200	71.36	0.71	1.12	1.12
$D$	...	0.64	0.34	...	...	0.71	0.31	0.45	0.97	0.80	0.97	0.80	0.97	0.97
$P$	...	0.032	0.620	...	...	0.012	0.718	0.254	0.000	0.003	0.000	0.003	0.000	0.000
CB_3_0_5_a	200	2	0	1.99	4.63	0.670	37.6	0.0088	153.9	0.166	64.28	0.67	1.15	1.15
CB_3_0_5_b	200	3	0	1.32	2.90	0.667	41.8	0.0044	84.9	0.198	48.58	0.78	1.09	1.09
CB_3_0_5_c	200	2	1	1.75	3.75	0.556	36.2	0.0056	126.2	0.176	55.00	0.80	1.07	1.06
CB_3_0_5_d	200	2	0	2.28	4.96	0.734	51.8	0.0141	101.6	0.221	71.79	0.67	1.15	1.15
CB_3_0_5_e	200	2	2	1.51	3.22	0.653	54.2	0.0051	65.9	0.197	56.79	0.80	1.08	1.08
$\bar{x}$	200	2.2	0.6	1.77	3.89	0.656	44.3	0.0076	106.5	0.192	59.29	0.74	1.11	1.11
$D$	...	0.64	0.50	...	...	0.74	0.32	0.34	0.97	0.80	0.97	0.80	0.97	0.97
$P$	...	0.032	0.155	...	...	0.008	0.669	0.596	0.000	0.003	0.000	0.003	0.000	0.000
CB_3_1/3_5_a	200	2	0	1.51	3.91	0.725	40.4	0.0043	235.5	0.245	85.71	0.61	1.21	1.21
CB_3_1/3_5_b	200	2	0	1.41	3.42	0.843	23.3	0.0017	811.3	0.185	75.00	0.68	1.14	1.14
CB_3_1/3_5_c	175	1	0	1.79	4.12	1.000	...	0.0011	$\infty$	0.181	86.07	0.64	1.17	1.17
CB_3_1/3_5_d	200	1	1	2.17	4.87	0.960	...	0.0053	1839.4	0.167	91.07	0.53	1.29	1.29
CB_3_1/3_5_e	100	1	0	1.75	4.56	1.000	...	0.0040	$\infty$	0.105	78.57	0.62	1.19	1.19
CB_3_1/3_5_f	200	1	2	1.63	3.96	0.957	...	0.0069	541.8	0.208	83.57	0.65	1.17	1.16

(continued on next page)

Table 2 (continued)

Run	$t$ (Myr)	$N_p$	$N_m$	$a_p/a_c^*$	$q_p/Q_B$	$S_m$	$S_s$	$S_d$	$S_c$	$S_r$	$m_1$ (%)	$E/E_0$	$L/L_0$	$L_Z/L_{Z_0}$
$\bar{x}$	179	1.3	0.5	1.71	4.14	0.914	37.6	0.0039	1184.5	0.182	83.33	0.62	1.19	1.19
$D$	...	0.77	0.54	...	...	0.90	0.38	0.58	0.97	0.83	0.97	0.83	0.97	0.97
$P$	...	0.002	0.069	...	...	0.000	0.365	0.043	0.000	0.001	0.000	0.001	0.000	0.000
CB_4_0_5_a	500	2	1	1.56	3.24	0.598	34.1	0.0011	153.3	0.206	67.15	0.67	1.16	1.16
CB_4_0_5_b	1000	1	2	1.34	2.73	0.971	...	0.0006	2183.7	0.141	75.00	0.72	1.11	1.11
CB_4_0_5_c	929	1	0	2.27	5.35	1.000	...	0.0214	$\infty$	0.081	90.00	0.57	1.23	1.22
CB_4_0_5_d	500	2	2	1.10	2.40	0.595	25.6	0.0024	193.0	0.281	85.00	0.71	1.12	1.12
CB_4_0_5_e	200	1	1	1.88	4.47	0.986	...	0.0008	3356.0	0.282	75.00	0.60	1.22	1.22
CB_4_0_5_f	129	1	0	1.99	5.46	1.000	...	0.0193	$\infty$	0.222	85.35	0.57	1.22	1.22
$\bar{x}$	543	1.3	1.0	1.69	3.94	0.858	32.7	0.0076	2099.7	0.202	79.58	0.64	1.18	1.17
$D$	...	0.77	0.27	...	...	0.81	0.64	0.67	0.97	0.74	0.97	0.83	0.97	0.97
$P$	...	0.002	0.795	...	...	0.001	0.017	0.011	0.000	0.004	0.000	0.001	0.000	0.000
MVEM	...	4.0	0.0	...	...	0.509	37.7	0.0018	89.9	...	...	...	...	...
SJS_ave	200	3.0	0.7	...	...	0.514	44.4	0.0157	40.5	0.420	25.92	1.26	0.87	0.87
Sun_ave	867	4.0	12.3	...	...	0.393	38.2	0.0318	15.9	0.360	0.48	1.06	1.01	1.00
Sun_ave ( $a < 2$ AU)	867	3.0	0.7	...	...	0.483	36.8	0.0061	34.3	...	18.66 <sup>b</sup>	1.21	0.90	0.90
$\alpha$ Cen A ( $i \leq 30^\circ$ )	481	3.9	0.2	...	...	0.432	38.4	0.0098	30.9	0.354	15.69	1.24	0.90	0.94

<sup>a</sup> Systems include ‘‘Jupiter’’ but not ‘‘Saturn.’’ All other simulations include both giant planets.

<sup>b</sup> Mass lost plus mass ending up in planets/minor planets beyond 2 AU.

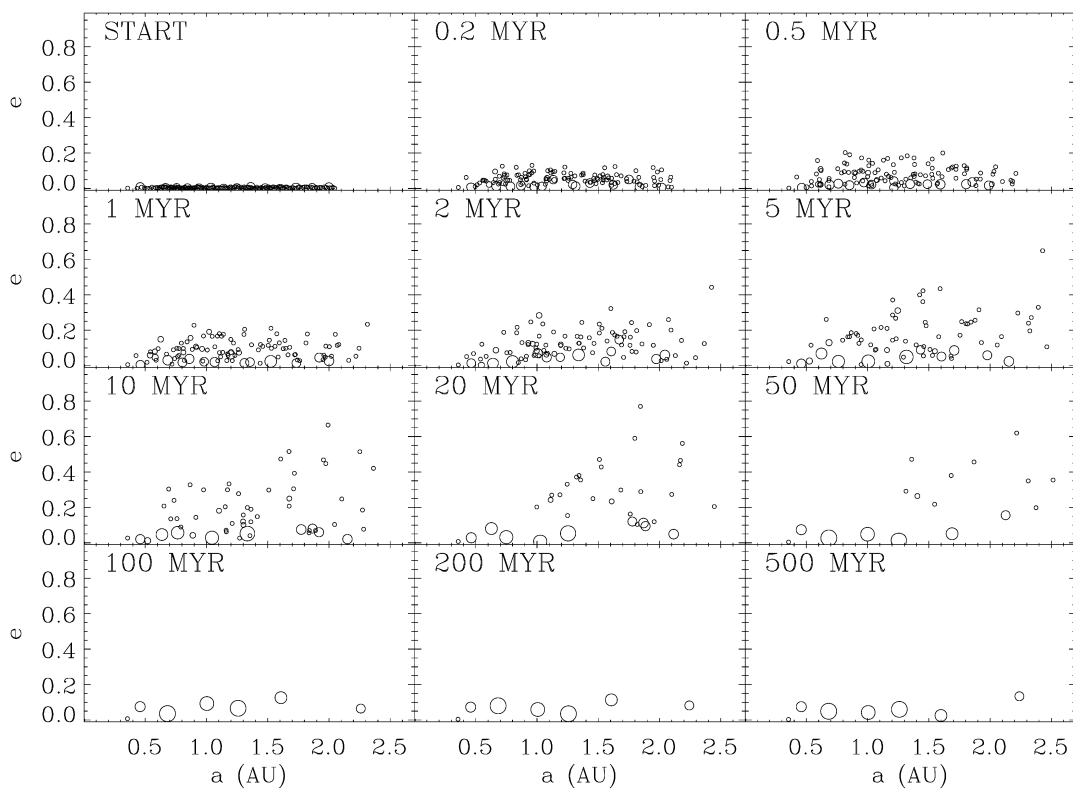


Fig. 1. The temporal evolution of the circumbinary disk in simulation CB\_05\_0\_5<sup>†</sup>\_a. For this simulation, the semimajor axis of the binary is  $a_B = 0.05$  AU, the binary orbit is circular ( $e_B = 0$ ) and each star has mass  $M_* = 0.5 M_\odot$ . A single, Jupiter-like, giant planet is also included. The planetary embryos and planetesimals are represented by circles whose sizes are proportional to the physical sizes of the bodies. The locations of the circles show the orbital semimajor axes and eccentricities of the represented bodies relative to center of mass of the binary stars. The initially dynamically cold disk heats up during the first 10 Myr, especially in the outer region, where the perturbations of the single giant planet included in this simulation are the greatest. By 93 Myr into the simulation, six planets on low eccentricity orbits have formed, with one planetesimal remaining interior to their orbits. All of these bodies survive for the remainder of the simulation.

planet growth around a single star with one or two giant planets (Chambers, 2001; Chambers et al., 2002; Appendix A) and around the individual stars in the  $\alpha$  Centauri AB binary, provided the disk begins close to the  $\alpha$  Cen binary orbital plane (Quintana et al., 2002, 2003).

Fig. 4 displays the evolution of CB\_075\_33\_5\_b, in which the stars orbit one another on more distant and eccentric paths. The system evolves very differently from any of the systems with  $a_B = 0.05$  and  $e_B = 0$ . The innermost large planet is quite eccentric by  $t = 20$  Myr, and it accretes or scatters all of the

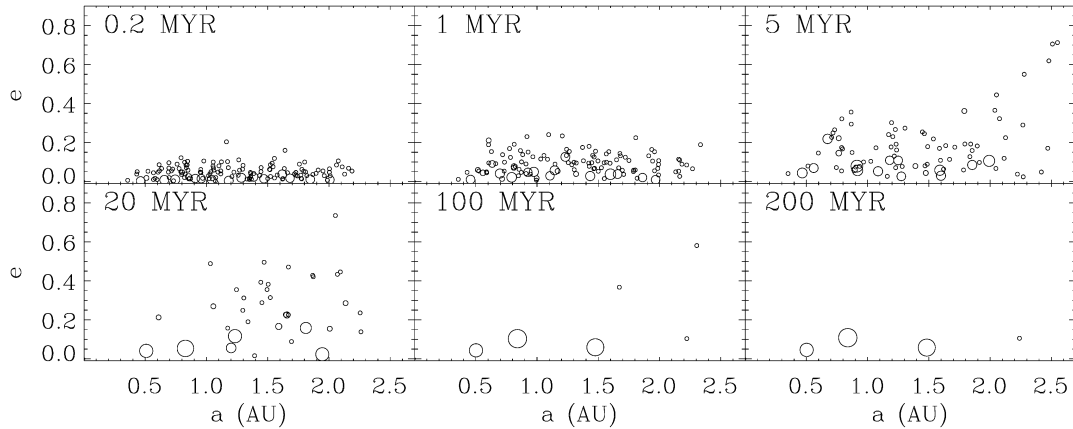


Fig. 2. The temporal evolution of simulation CB\_05\_0\_5<sup>†</sup>\_d. The masses and initial parameters of all bodies are identical to those used in the simulation displayed in Fig. 1, aside from the shift of one planetesimal 3 m forward along its orbit. Thus, the initial masses, semimajor axes and eccentricities are the same as those shown in the first panel of Fig. 1. The meanings of the symbols are as described in the caption to Fig. 1. Note that while this system seems qualitatively similar to the one represented in Fig. 1 at early times, in this case only three terrestrial-mass planets survive.

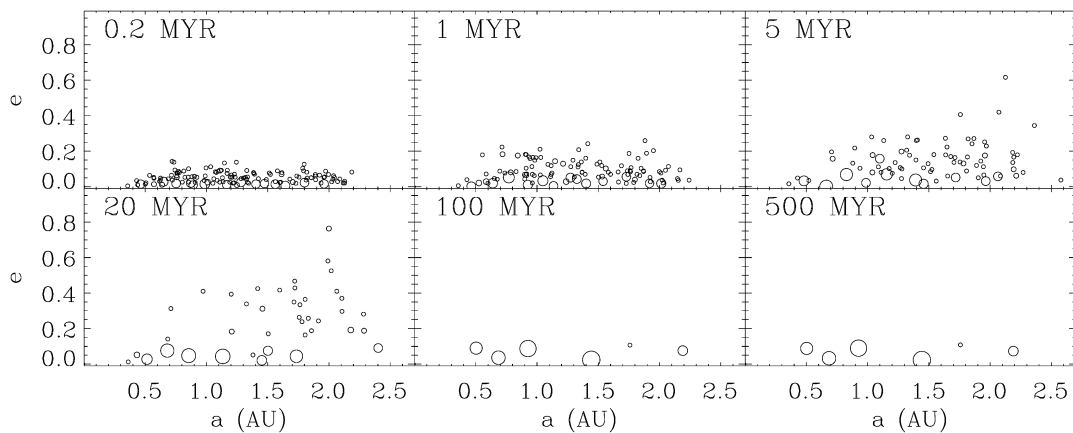


Fig. 3. The temporal evolution of simulation CB\_05\_0\_5\_c, which included both “Jupiter” and “Saturn.” Despite the addition of a second giant planet, the development of the system appears to be intermediate between the systems displayed in the previous two figures. See the first panel in Fig. 1 for the initial conditions and the caption of Fig. 1 for an explanation of the symbols.

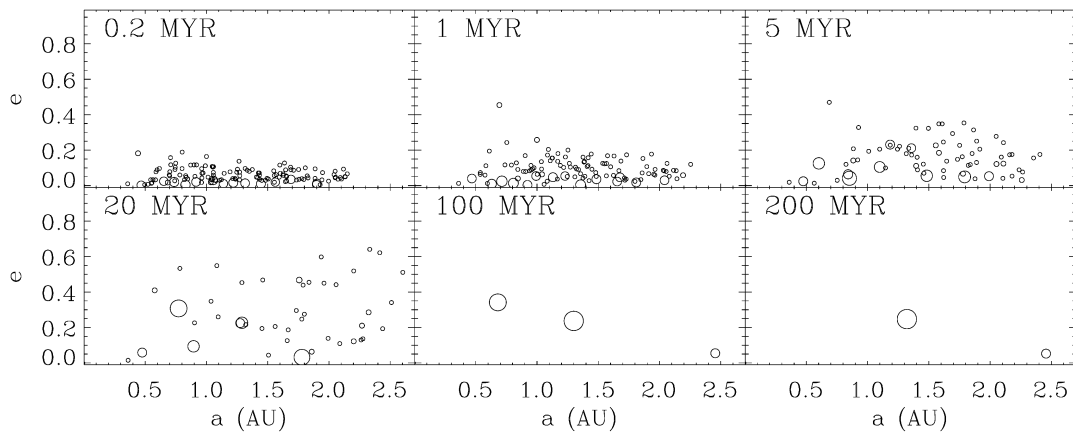


Fig. 4. The temporal evolution of simulation CB\_075\_33\_5\_b. The larger binary semimajor axis ( $a_B = 0.075$  AU) and eccentricity ( $e_B = 0.33$ ) produce greater perturbations on the disk than those occurring in the systems shown in the previous figures. The protoplanetary system is much more dynamically excited, especially in the inner regions, and a substantial amount of material is ejected, leaving only two planets. See the first panel in Fig. 1 for the initial conditions and the caption of Fig. 1 for an explanation of the symbols.

smaller bodies inwards of 1 AU prior to being ejected itself at 106 Myr. Run CB\_075\_33\_5\_d produces a similar planetary

system, whereas runs CB\_075\_33\_5\_a, CB\_075\_33\_5\_c, and CB\_075\_33\_5\_e result in planetary systems resembling

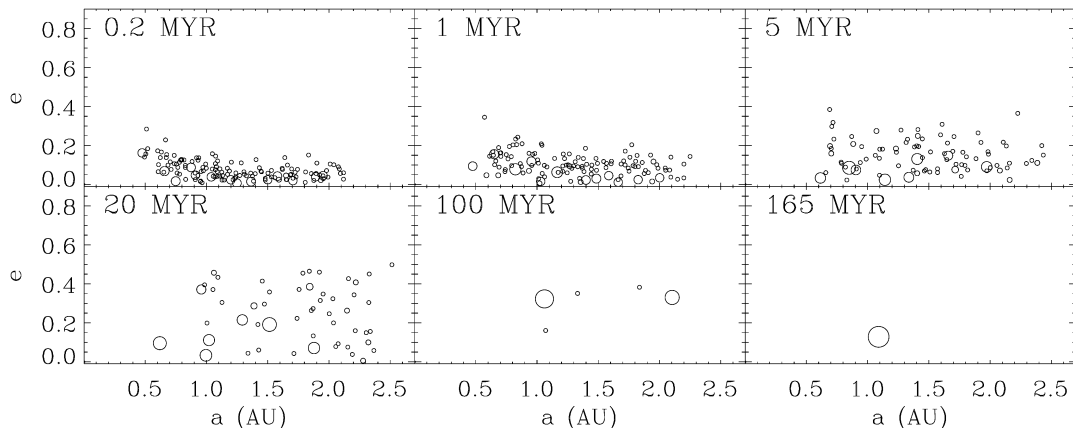


Fig. 5. The temporal evolution of simulation CB\_1\_8\_2\_d. The effect of a larger stellar separation ( $a_B = 0.1$  AU) and higher binary eccentricity ( $e_B = 0.8$  AU), compared with previous figures, is apparent in the first panel where the inner part of the disk is already substantially excited by 200,000 yr. Eccentricities remain high throughout the evolution, and by 164 Myr only one body remains in the terrestrial planet zone. See the first panel in Fig. 1 for the initial conditions and the caption of Fig. 1 for an explanation of the symbols.

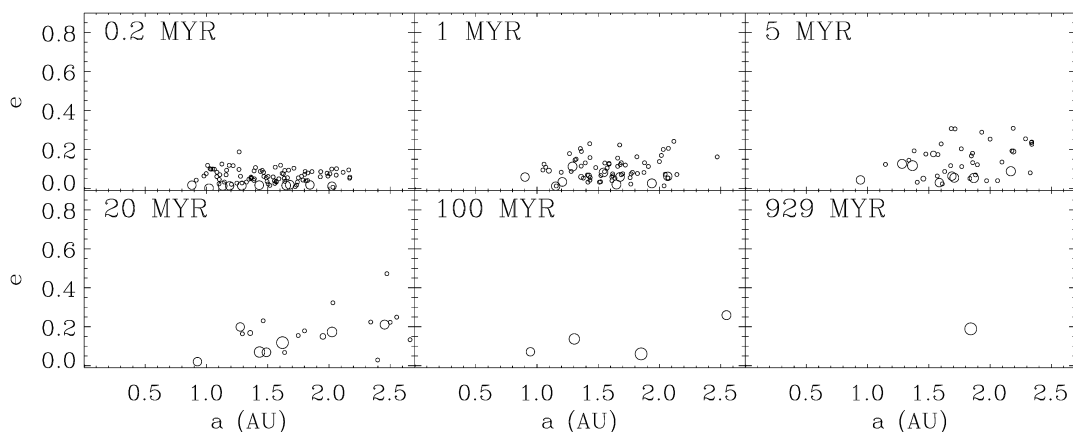


Fig. 6. The temporal evolution of simulation CB\_4\_0\_5\_c. With the binary on a circular orbit with semimajor axis equal to 0.4 AU, the inner part of the disk is cleared out to beyond 0.8 AU by 200,000 yr. The system of four smallish planets that formed beyond 0.9 AU by 100 Myr looks as if it might be stable. However, the outermost planet was ejected at 110 Myr. The remaining planets continued to interact until the orbits of the inner two planets crossed, resulting in the ejection of the innermost planet near 1 AU at 775 Myr. The planet near 1.3 AU was ejected at 929 Myr, leaving just one body orbiting at 1.8 AU. See the first panel in Fig. 1 for the initial conditions and the caption of Fig. 1 for an explanation of the symbols.

those formed in the  $a_B = 0.05$  and  $e_B = 0$  simulations (Table 2 and Fig. 8). In a sense, this change in stellar parameters yields systematic differences comparable to the scatter resulting from chaos.

Figs. 5 and 6 show the evolution of systems CB\_1\_8\_2\_d and CB\_4\_0\_5\_c, respectively. In each case, the binary apastron distance is much larger than in the runs discussed above, and binary perturbations clear the system of all but one planet. Additional planets remain in the runs with nearly identical initial parameters, but the systems (Table 2, Figs. 7 and 8) still look much sparser, especially in the inner regions, than those formed around a single star, very close binaries, or individual stars in the  $\alpha$  Cen AB system. In these cases, systematic effects resulting from the different binary parameters exceed typical chaotic variations. Figs. showing the temporal evolution of most of the simulations discussed in this paper are presented in Quintana (2004); plots of simulations CB\_1\_0\_5\_c and CB\_2\_5\_5\_a are presented in Lissauer et al. (2004).

Figs. 7 and 8 show the final planetary systems formed in all of our simulations. The top left row in each figure shows

the Solar System’s terrestrial planets (labeled ‘MVEM’), followed by the 5–6 realizations of each binary system under study, presented in order of increasing  $Q_B$ . Fig. 7 presents the final planetary systems formed around binary stars that began on circular orbits with the disk initially coplanar to the stellar orbit (labeled in the following format:  $a_B e_B \mu$ ), whereas Fig. 8 shows the results for simulations with  $i = 30^\circ$  and the sets of runs with  $e_B > 0$ . In these figures, the radius of each body is proportional to the radius of the planet that it represents, the horizontal lines through each body indicate the periastron and apastron distances to the center of mass of the binaries (or the Sun in the MVEM case), the vertical lines represent the inclination relative to the binary orbital plane (the Laplacian plane in the MVEM case), and the arrows show the orientation of the final spin axes of each planet (arrows are omitted for planetesimals and embryos that survived the integration without a collision). Although the final planetary systems formed vary widely among a given set of binary star parameters due to the chaotic nature of these simulations, general trends are apparent in the planets formed around stars with larger separations and

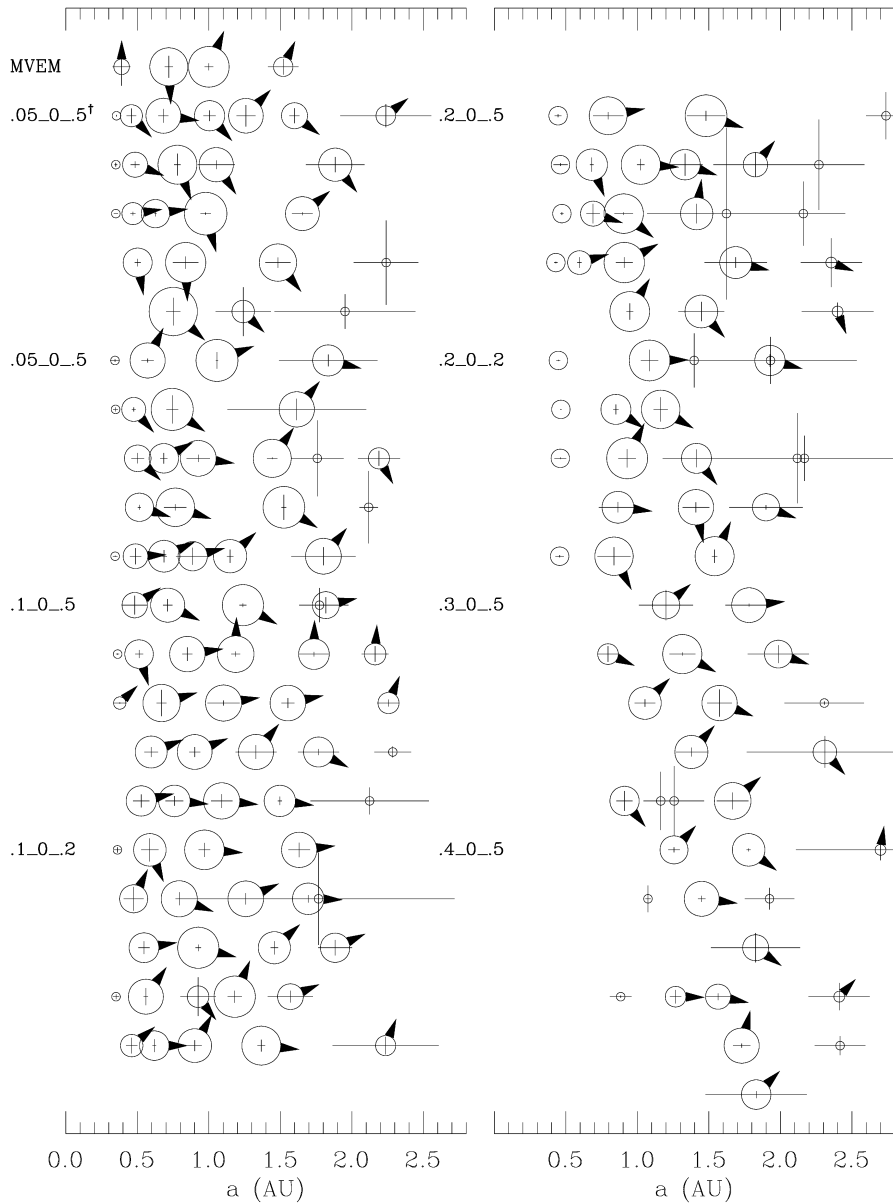


Fig. 7. This figure displays the final planetary systems formed in all simulations which begin with binary stars on circular orbits ( $e_B = 0$ ) and with the initial disk coplanar with the stellar orbit. Symbol sizes are proportional to planet sizes, the centers of the circles are positioned horizontally at the planet's semimajor axis, the horizontal bar represents the extent of the planet's radial excursions, and the vertical bar (which is proportional to the planet's inclination) shows its out of plane motion. All orbital parameters are computed relative to the center of mass of the binary star system. Arrows point in the direction representing the planet's rotational angular momentum; bodies that did not accrete do not have arrows attached because we have no information regarding their obliquity. The terrestrial planets in our Solar System are shown in the upper left. Modeled systems are grouped by common binary star parameters. Note the diversity caused by chaos within individual groups, and also the general trends with increases in binary semimajor axis. Also note that an additional planetesimal (which is not shown in this figure) remains in the third planetary system of set\_2\_0\_2 (simulations CB\_2\_0\_2\_c) at  $a_p = 2.98$  AU,  $e_p = 0.18$  AU, and  $i_p = 4.3^\circ$  relative to the binary orbital plane.

higher eccentricities. In order to quantitatively analyze these effects, we developed a set of formulae that characterize the orbits and distribution of mass for all of the final planetary systems. These are described in the next subsection and the statistical variations are discussed in Section 4.2.

#### 4.1. Parameters and statistics

The results of all of our close binary simulations are given in Table 2, which lists the stellar parameters/initial conditions and gives the values of statistical parameters that were devel-

oped to help characterize the final planetary systems. Most of these statistics were previously used to compare the outcomes from accretion simulations in the Sun–Jupiter–Saturn (SJS) system (Chambers, 2001; Appendix A) and around each star in the  $\alpha$  Cen AB binary star system (Quintana et al., 2002, 2003), all of which used essentially the same initial planetesimal disk. The first column lists the name of each close binary simulation (CB\_ $a_B$ \_ $e_B$ \_ $\mu$ \_ $x$ , as described in Section 2). Simulations that include just one giant planet (Jupiter) are labeled with  $\dagger$ ; all others include a Jupiter-like planet and a Saturn-like planet. When the initial midplane of the circumbinary disk is inclined relative

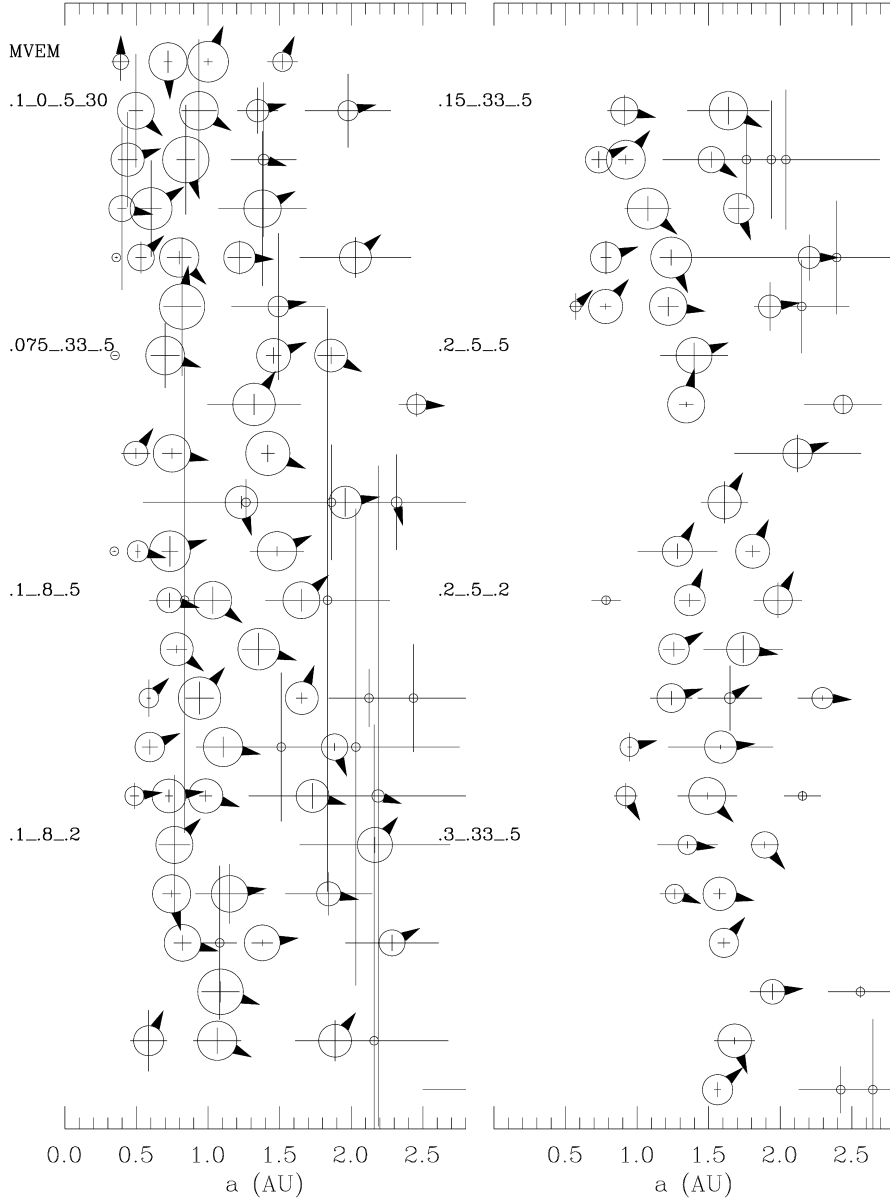


Fig. 8. This figure displays the final planetary systems for the set of runs in which the disk was initially inclined by  $30^\circ$  (labeled ‘.1\_0\_5\_30’), and the simulations which begin with binary eccentricities  $e_B > 0$  (presented in order of increasing apastron  $Q_B$ ). Symbols are explained in the caption to Fig. 7. Note that the planetary systems shown here generally are sparser and more diverse than those computed for binary stars on circular orbits (Fig. 7), but that again there is a wide range of outcomes due to the chaotic nature of planetary accretion dynamics.

to the stellar orbit, the runs are denoted  $CB_{a_B}e_B\mu_i_x$ . The duration of each simulation is listed in column 2. Columns 3–15 present the following statistics [see Chambers (2001) and Quintana et al. (2002) for mathematical descriptions of the statistics given in columns 7–15; statistics presented in columns 5 and 6 are new in this work].

- (3) The number of planets,  $N_p$ , that are at least as massive as the planet Mercury ( $\sim 0.06 M_\oplus$ ). Note that the 14 planetary embryos in the initial disk each satisfy this mass requirement, as do bodies consisting of at least 7 planetesimals.
- (4) The number of minor planets,  $N_m$ , that are less massive than the planet Mercury.
- (5) The ratio of the semimajor axis of the innermost final planet to the closest stable orbit of the system,  $a_p/a_c^*$ . Note that in principle, the value of this quantity may be (slightly) less than unity, as  $a_c^*$  was estimated using a coarse grid and only considered bodies initially on circular orbits within the binary plane.
- (6) The ratio of the periastron of the innermost final planet,  $q_p = a_p(1 - e_p)$ , to the binary apastron  $Q_B = a_B(1 + e_B)$ .
- (7) The fraction of (the final) mass in the largest planet,  $S_m$ .
- (8) An orbital spacing statistic,  $S_s$ , which gives a measure of the distances between the orbits of the final planets (that are larger than the planet Mercury). Larger values of  $S_s$  imply more widely spaced final planets.

- (9) The normalized angular momentum deficit,  $S_d$ , which measures the fractional difference between the planets' actual orbital angular momenta and the angular momenta that they would have on circular, uninclined orbits with the same semimajor axes.
- (10) A mass concentration statistic,  $S_c$ , which measures the degree to which mass is concentrated in one part of the planetary system.
- (11) A radial mixing statistic,  $S_r$ , which sums the radial migrations of the bodies that form a planet.
- (12) The percentage of the initial mass that was lost from the planetary system (came too close to the stars or was ejected to interstellar space),  $m_1$ .
- (13) The total mechanical (kinetic + potential) energy per unit mass for the planets remaining at the end of a simulation,  $E$ , normalized by  $E_0$ , the energy per unit mass of the system prior to the integration.
- (14) The angular momentum per unit mass of the final planets,  $L$ , normalized by  $L_0$ , the angular momentum per unit mass of the initial system.
- (15) The  $Z$  component of angular momentum per unit mass relative to the stellar orbit,  $L_Z$ , normalized by  $L_{Z_0}$ , the initial  $Z$  component of angular momentum of the system.

Following the close binary results in Table 2 are analogous statistics for the following systems: the four terrestrial planets in the Solar System (labeled 'MVEM'); the averaged values for 31 accretion simulations in the Sun–Jupiter–Saturn system ('SJS\_ave,' which are presented in Appendix A); the averaged values of a set of accretion simulations around the Sun with neither giant planets nor a stellar companion perturbing the system ('Sun\_ave,' Quintana et al., 2002; Appendix A); the averaged values for the planets formed within 2 AU of the Sun when neither giant planets nor a stellar companion is included ('Sun\_ave ( $a < 2$  AU),' Quintana et al., 2002; Appendix A); and the averaged values for the planetary systems formed around  $\alpha$  Cen A in simulations for which the accretion disk began with an inclination  $i \leq 30^\circ$  to the  $\alpha$  Cen AB binary orbital plane (labeled ' $\alpha$  Cen ( $i \leq 30^\circ$ ),' Quintana et al., 2002). Note that only the six statistics listed for the terrestrial planets in our Solar System (MVEM) are actual observables.

We use a two-sided Kolmogorov–Smirnov (KS) test to compare each planetary statistic for each binary star configuration to the analogous planetary statistic from the distribution of 31 SJS simulations (Appendix A). Table 2 gives the KS statistic,  $D$ , and the associated probability,  $P$ , for each set of simulations. Generally, values of  $P \lesssim 0.05$  indicate that the two sets of data are drawn from different distribution functions, i.e., the effect of the binary stars on the disk is statistically significant. The orbital spacing statistic,  $S_s$  (column 8 in Table 2), is undefined in simulations which resulted in the formation of a single planet ( $N_p = 1$ , including those systems with  $N_m \neq 0$  since these smaller bodies are neglected for this calculation). Simulations with  $N_p = 1$  and  $N_m = 0$  have an infinite value for the mass concentration statistic,  $S_c$  (column 10 in Table 2). In each case, when calculating  $D$  and  $P$ , the values for these statistics are replaced by the highest finite value of the statis-

tic within that set of runs in order to minimize biasing of the results. The results from Table 2 are discussed in the next subsection.

#### 4.2. Statistical variations among the systems

Nearly all of the simulations that began with binary stars with  $Q_B \leq 0.2$  AU resulted in distributions of planetary systems that are statistically consistent in most properties with those formed in the SJS simulations. The mass loss, final specific energy, and final specific angular momentum statistics for the close binary simulations (columns 12–15 in Table 2), however, differ from the corresponding SJS distributions, and will be discussed later in this section. One set of simulations (the CB\_1\_0\_5 runs) in which 4–5 terrestrial-mass planets formed (compared to an average of 3 planets formed in the SJS runs) have planetary statistics that are inconsistent with the SJS distributions, even though the final planets have masses and orbits that appear upon inspection to be similar to the terrestrial planets in our Solar System. This divergence is possible because the statistical tests are of marginal use for comparing ensembles with only five members. We include the statistics because they provide a different, albeit not necessarily better, perspective from a visual comparison of the final systems shown in Figs. 7 and 8.

Neglecting to include a Saturn-like planet in addition to the Jupiter-like planet in the simulations did not affect the final outcomes of the planets in a statistically significant manner. The first two sets of runs listed in Table 2 ( $a_B = 0.05$ ) show that the effects of chaos are larger than the effects from the number of giant planets that are included. Nonetheless, it is worth noting that the most crowded final system, run CB\_05\_0\_5<sup>†</sup>\_a, in which 6 planets and 1 planetesimal survived, was subject to the perturbations of only a single giant planet.

One surprising result is that one run ended with 6 terrestrial planets and five runs concluded with 5 planets. In all of these runs, the binary stars' mutual orbit was circular with  $a_B = 0.05, 0.1, \text{ or } 0.2$  AU. In contrast, at most 4 planets remained in the single star simulations listed in Table 3. Within each set of close binary simulations, at least one planet more massive than the planet Mercury remained in an orbit farther from the center of mass of the system than the present orbit of Mars ( $\sim 1.5$  AU). In many of the close binary simulations, Mars-sized planets formed (and/or planetesimals remained) in orbits beyond  $\sim 2$  AU from the center of mass of the binary stars. In our Solar System and in the SJS simulations, the location of the  $\nu_6$  secular resonance restricts terrestrial planet formation to within  $\sim 2$  AU of the Sun. In contrast, orbital precession induced by the binary displaces secular resonances of the giant planets away from the terrestrial planet zone. We integrated test particles orbiting 1.5–2.5 AU from a single or close binary star that had Jupiter and Saturn-like planetary companions. The eccentricities excited in the test particles orbiting the single star reached substantially higher values than did those of test particles around the binary, consistent with expectations.

The variations in the orbital elements of Jupiter and Saturn are larger in most of the close binary simulations compared

to simulations with a single star. In the SJS set, the average peak to trough variations of Jupiter’s semimajor axis, eccentricity, and inclination are  $\Delta a_{\text{J}} \sim 0.006$  AU,  $\Delta e_{\text{J}} \sim 0.038$ , and  $\Delta i_{\text{J}} \sim 0.32^\circ$ , respectively. For Saturn, these variations are  $\Delta a_{\text{S}} \sim 0.077$  AU,  $\Delta e_{\text{S}} \sim 0.086$ , and  $\Delta i_{\text{S}} \sim 0.785^\circ$ . In the close binary simulations, the average peak to trough variations in semimajor axes and eccentricities for both Jupiter and Saturn are slightly larger (although the changes are more chaotic in systems with larger  $Q_{\text{B}}$ ), with  $\Delta a_{\text{J}} \sim 0.01$  AU,  $\Delta e_{\text{J}} \sim 0.06$ ,  $\Delta a_{\text{S}} \sim 0.14$  AU, and  $\Delta e_{\text{S}} \sim 0.11$ . The variations in inclination increase with increasing  $Q_{\text{B}}$  for both Jupiter (up to  $2.3^\circ$ ) and Saturn (up to  $3.5^\circ$ ).

In the majority of simulations that began with binary stars on circular orbits and  $a_{\text{B}} \leq 0.2$  AU, the terrestrial planet systems that formed span essentially the entire range of the initial disk. The stellar perturbations on the inner edge of the disk become apparent in simulations with  $Q_{\text{B}} \geq 0.3$  AU and in many of the simulations with smaller  $Q_{\text{B}}$  but  $e_{\text{B}} > 0$  (Figs. 7 and 8). The statistics in columns 5 and 6 of Table 2 give a measure of how close the innermost planet forms to the innermost stable orbit of the system,  $a_{\text{p}}/a_{\text{c}}^*$ , and the ratio of the closest approach of the planet to the binary apastron,  $q_{\text{p}}/Q_{\text{B}}$ . These statistics do not have analogs in the SJS system, but are useful in comparing simulations with differing binary star parameters. Note that for most final systems,  $q_{\text{p}}/Q_{\text{B}} \sim 2a_{\text{p}}/a_{\text{c}}^*$ . In the first two sets of simulations ( $a_{\text{B}} = 0.05$  AU), the stars have a minimal effect on the inner edge of the disk, which begins at more than 3.5 times the distance (from the center of mass of the binary stars) of the location of the innermost stable orbit of the system,  $a_{\text{c}}^*$ . In more than one-third of the simulations with  $Q_{\text{B}} \leq 0.1$  AU (all of which use  $e_{\text{B}} \leq 1/3$  and have  $a_{\text{c}}^* \lesssim 0.2$  AU), the innermost planetesimal in the initial disk survived the entire integration without a collision and remained close to its initial orbit at  $\sim 0.35$  AU (Figs. 7 and 8). In eight of the ten simulations with  $a_{\text{B}} = 0.2$  and  $e_{\text{B}} = 0$ , the innermost embryo survived the integration without a collision. Binary systems with  $Q_{\text{B}} \geq 0.18$  AU have larger values of  $a_{\text{c}}^*$  ( $0.32$  AU  $< a_{\text{c}}^* < 0.9$  AU) that approach or exceed the initial orbit of the innermost body in the protoplanetary disk. Although the inner edge of the disk is truncated, the innermost planets formed in many of these simulations remain on orbits that are close to the system’s  $a_{\text{c}}^*$ .

In the SJS set of simulations and in the CB\_05\_0\_5<sup>†</sup> runs, an average of  $\sim 51\%$  of the mass that composes the final planets remained in the largest planet formed, the same fraction of mass that composes the Earth in the Mercury–Venus–Earth–Mars system. The value of  $S_{\text{m}}$  (the fraction of final mass that composes the largest planet) is generally higher in the close binary simulations that resulted in fewer planets. With the exception of two sets of runs (the CB\_1\_0\_5 set with an average value of  $S_{\text{m}} = 0.35$ , and the CB\_15\_1/3\_5 set with an average of  $S_{\text{m}} = 0.64$ ), all of the sets of simulations with  $Q_{\text{B}} \leq 0.2$  AU have values of  $S_{\text{m}}$  that are statistically consistent with those in the SJS set of runs (typically  $\sim 0.5$ ). The value of  $S_{\text{m}}$  tends to be larger for planets that form around more eccentric binary stars, yet the effect of varying the stellar mass ratio for systems with common  $a_{\text{B}}$  and  $e_{\text{B}}$  appears to be statistically insignificant.

The statistic  $S_{\text{s}}$ , which quantifies the orbital spacing of the final planets, ranged from 29–87 (with an average of 44) in the SJS distribution, and is  $S_{\text{s}} = 38$  for the terrestrial planets in the Solar System. The CB\_1\_0\_5 simulations resulted in a higher number of planets that were more closely spaced, with  $S_{\text{s}} = 32$  on average. All other sets of close binary simulations with  $Q_{\text{B}} \leq 0.2$  AU resulted in planetary systems with  $S_{\text{s}}$  values that are consistent with the  $S_{\text{s}}$  distribution of the SJS set. Note that one-fourth of the simulations of binary stars with  $Q_{\text{B}} \geq 0.3$  AU produced only a single terrestrial planet,  $N_{\text{p}} = 1$ , in which case  $S_{\text{s}}$  is omitted. If we consider only SJS and close binary simulations which resulted in  $N_{\text{p}} \geq 3$  (since two planet systems generally give high values of this statistic), then the SJS distribution has an average value of  $S_{\text{s}} = 38$ , the same as the Solar System’s terrestrial planets. Comparing this limited distribution of  $S_{\text{s}}$  to close binary simulations (again omitting 2 planet systems) with  $Q_{\text{B}} \leq 0.2$  AU (nearly all simulations with larger  $Q_{\text{B}}$  resulted in 1 and 2 planet systems), we again find that only the CB\_1\_0\_5 set results in a statistically different (lower) value of  $S_{\text{s}}$  than the SJS  $N_{\text{p}} \geq 3$  distribution.

The angular momentum deficit ( $S_{\text{d}}$ ), which measures the orbital excitation of a planetary system, is an order of magnitude larger for the set of planet systems that formed in the SJS simulations ( $S_{\text{d}} = 0.02$ , on average) than for the Solar System terrestrial planets ( $S_{\text{d}} = 0.002$ ). Most of the planetary systems that formed around close binaries with  $Q_{\text{B}} \leq 0.3$  AU (in simulations in which the midplane of the disk began coplanar to the stellar orbit) have values of  $S_{\text{d}}$  that are on average comparable to the SJS distribution. The exceptions are the two sets of simulations with  $a_{\text{B}} = 0.1$  and  $e_{\text{B}} = 0$ , both of which have smaller values of  $S_{\text{d}}$  (but even these sets have higher angular momentum deficit than do the actual terrestrial planets in our Solar System). The relatively high values of final planetary eccentricities and inclinations are a well known difficulty of models of the late stages of terrestrial planet growth within our Solar System (Agnor et al., 1999; Chambers, 2001).

The radial distribution of mass in the final planetary systems is measured herein by the mass concentration statistic,  $S_{\text{c}}$ . In the Solar System,  $\sim 90\%$  of the mass of the terrestrial planets is concentrated in Venus and in Earth ( $S_{\text{c}} = 90$ ). With the exception of the simulations which resulted in a single planet (for which this value is infinite),  $S_{\text{c}}$  ranged from 21 to 81 (with an average of  $S_{\text{c}} = 40$ ) in the SJS set of runs. In all of the close binary simulations that ended with  $N_{\text{p}} \geq 3$ ,  $S_{\text{c}}$  ranged from 25 to 85. For most of the two-planet systems,  $S_{\text{c}}$  had much higher values, especially in systems with  $Q_{\text{B}} > 0.2$  AU.

The degree of radial mixing,  $S_{\text{r}}$ , which sums the radial migrations of the bodies that form a final planet, is not known for our Solar System, but has an average value of  $S_{\text{r}} = 0.42$  for the SJS planetary systems. The values of  $S_{\text{r}}$  are more widely varied among each close binary set. As  $Q_{\text{B}}$  is increased and more mass is lost, the degree of radial mixing is reduced, and the sets of simulations with  $Q_{\text{B}} \geq 0.2$  AU have smaller values of  $S_{\text{r}}$  by a statistically significant amount than do simulations around a single star.

The percentage of mass that was lost in most of the close binary sets of simulations is statistically inconsistent with the average total mass loss in the SJS set of runs ( $m_1 \sim 26\%$ ). Simulations with binary stars on circular orbits with  $a_B \leq 0.1$  AU resulted in planetary systems that accreted, on average, more of the initial disk mass ( $m_1 \sim 15\text{--}18\%$ ) than the SJS runs, which can be attributed to both the relatively weak stellar perturbations on the inner edge of the disk compared to the other binary star systems, and to the lack of secular resonances from the giant planets near the outer edge of the disk, which are an important source of perturbations in the SJS systems. The amount of mass lost in the close binary simulations was typically much higher in systems with larger  $Q_B$ , and only the CB\_075\_1/3\_0.5 set and the CB\_2\_0\_0.5 set resulted in a comparable amount of mass loss as the SJS runs, as did the set which began with the midplane of the disk inclined by  $30^\circ$  to the binary orbital plane, CB\_1\_0\_0.5\_30°. More mass was lost and fewer planets were formed (on average) when the stellar masses were unequal ( $\mu = 0.2$ ), since binaries with more extreme mass ratios (smaller  $\mu$ ) travel farther from the center of mass of the pair.

In addition to the differences in mass loss, all of the close binary simulations that began with the disk coplanar to the stellar orbit resulted (on average) in smaller values of the specific energy ( $E/E_0$ ), and greater values of the specific angular momentum ( $L/L_0$ ) and specific  $Z$ -component of angular momentum ( $L_Z/L_{Z_0}$ ). This is also probably related to the clearing of the region near 2 AU by the  $\nu_6$  resonance in the SJS system. In close binary systems with  $Q_B \geq 0.2$  AU, the final specific energy was higher than (or comparable to) the system's initial specific energy ( $E/E_0 \gtrsim 1$ ), although still not as high as the average value of  $E/E_0$  for the SJS runs ( $\sim 1.26$ ). As  $a_B$  and/or  $e_B$  is increased, and planets form farther from the binary center of mass, the specific energy decreases (even to as low as 50% of the system's initial specific energy) while the changes in angular momenta increase by as much as 30%.

The simulations that began with the midplane of the disk inclined relative to the stellar orbit, CB\_1\_0\_0.5\_30°, were the only set that resulted in a greater average value of  $E/E_0$  and a smaller average  $L/L_0$  than the SJS runs. These are both consequences of the inward drift of the disk resulting from the initial tilt of the disk to the binary orbital plane. Even larger manifestations of this effect are evident in the high-inclination simulations of terrestrial planet formation within the  $\alpha$  Centauri AB system (Quintana et al., 2002). The amount of mass loss (an average of 25%), the average specific energy, and the average specific angular momentum are statistically consistent with the SJS simulations, but this is simply a result of the coincidental cancellation of greater inward motion and the absence of the  $\nu_6$  resonance. However, the  $Z$ -component of angular momentum had values that were smaller than in the SJS simulations, because the final systems have similar total angular momentum yet larger inclinations (which also lead to a statistically significant increase of the angular momentum deficit,  $S_d$ ).

## 5. Summary and conclusions

In the present work, we have examined the effect of 14 different short-period binary star configurations (each with a combined stellar mass of  $1 M_\odot$ ) on the late stages of terrestrial planet formation within a circumbinary protoplanetary disk. Stellar mass ratios of 1:1 and 4:1 were examined, and the initial orbits of the stars were varied (with semimajor axes between  $0.05 \text{ AU} \leq a_B \leq 0.4 \text{ AU}$  and eccentricities  $e_B \leq 0.8$ ) such that the stellar apastron ranged from  $0.05 \text{ AU} \leq Q_B \leq 0.4 \text{ AU}$ . The midplane of the disk began coplanar to the stellar orbit in all but one set of runs; in that exceptional set, the initial inclination of the disk started at  $30^\circ$  relative to the binary orbital plane. Giant planets analogous to Jupiter (at  $\sim 5.2 \text{ AU}$ ) and, in all but one set of runs, Saturn (at  $\sim 9.5 \text{ AU}$ ) were included. The evolution of the protoplanets was followed using a symplectic ‘close binary’ algorithm which was developed for this purpose (Chambers et al., 2002), and 5 or 6 simulations were performed for each binary star system under study (with small changes in the initial conditions of the disk) to account for the chaotic nature of these  $N$ -body systems. We statistically compared our results to a large set of simulations of the Sun–Jupiter–Saturn system that began with virtually the same initial disk mass distribution [initially performed by Chambers (2001), but also integrated herein (Appendix A)].

The close binary stars with maximum separations  $Q_B \equiv a_B(1 + e_B) \leq 0.2 \text{ AU}$  and small  $e_B$  had little effect on the accreting bodies, and in most of these simulations terrestrial planets formed over essentially the entire range of the initial disk mass distribution (and even beyond 2 AU in many cases). The stellar perturbations cause orbits to precess, thereby moving secular resonances out of the inner asteroid belt, allowing terrestrial planets to form from our initially compact disk and remain in stable orbits as far as 2.98 AU from the center of mass of the binary stars.

The effect of the stellar perturbations on the inner edge of the planetesimal disk become evident in systems with larger  $a_B$  (and  $Q_B \geq 0.3 \text{ AU}$ ) and in most of the simulations with  $e_B > 0$ . Terrestrial-mass planets can still form around binary stars with nonzero eccentricity, but the planetary systems tend to be sparser and more diverse. Binary stars with  $Q_B \geq 0.3 \text{ AU}$  perturb the accreting disk such that the formation of Earth-like planets near 1 AU is unlikely. Despite these constraints, at least one terrestrial planet (at least as massive as the planet Mercury) formed in each of our simulations.

## Acknowledgments

We thank John Chambers for performing additional simulations presented in Appendix A. Fred Adams, John Chambers, and two anonymous referees provided informative suggestions which helped us improve the manuscript. This research was supported in part by an Astrobiology Grant (21-344-53-1y) and a grant from the NASA Ames Director's Discretionary Fund. E.V.Q. is a NAS/NRC, and she was supported in the early stages of this research by a NASA Graduate Student Researchers Pro-

gram Fellowship and a Michigan Center for Theoretical Physics Fellowship.

## Appendix A. Terrestrial planet formation in the Sun–Jupiter–Saturn system

The initial conditions of the circumbinary disk used in our close binary simulations are taken from an earlier study of terrestrial planet formation within a disk around the Sun with Jupiter and Saturn perturbing the system (Chambers, 2001). In a set of 16 accretion simulations, Chambers (2001) varied the initial mass distribution of the circumstellar disk with the intent of determining which conditions best resulted in the formation of terrestrial planets with masses and orbits similar to those in the Solar System. Approximately 150 rocky bodies (with a total disk mass  $\approx 2.5 M_{\oplus}$ ) were placed between 0.3 and 2 AU of the Sun, with a surface density that is consistent with the minimum mass model of the solar nebula (Weidenschilling, 1977). The masses of the bodies in the disk began with either a uniform or a ‘bi-modal’ distribution (in which half of the disk mass is divided into Mars-sized planetary embryos that are embedded in a swarm of lunar-sized planetesimals). The radius of each body was calculated assuming a material density of  $3 \text{ g cm}^{-3}$ . The disk was initially placed in the invariable plane of Jupiter and Saturn, and each system was evolved forward in time for  $\sim 150\text{--}300$  Myr.

Two simulations, labeled ‘J21’ and ‘J22’ in Chambers (2001), were the most successful in reproducing terrestrial planets similar to those in the Solar System. Each of these began with the bi-modal mass distribution, and differed only in their randomly chosen initial arguments of perihelion, longitudes of the ascending node, and mean anomalies of the embryos and planetesimals. We chose to use the initial disk mass distribution from the J21 run for all of our close binary simulations in order to delineate the effects of an inner binary star system from the perturbations of a single star (i.e., varying the initial disk mass distribution in addition to examining the enormous binary star parameter space is computationally intensive).

To examine the statistical differences between planets formed around close binaries and those formed around the Sun, we performed an additional 27 simulations of the Sun–Jupiter–Saturn system (using conditions nearly identical to the J21 and J22 integrations) to provide a larger distribution of final planetary systems that form around the Sun. Table 3 presents the planetary statistics (as described in Section 4.1) for all of the SJS simulations. In Group 1, the original *Mercury* hybrid symplectic algorithm (Chambers, 1999) was used. Group 1a lists the planetary statistics for the original J21 and J22 simulations of Chambers (2001). The next two groups each begin with the same initial conditions as J21 (Group 1b) or J22 (Group 1c), with the exception of a small shift in the initial mean anomaly of one planetesimal by 1–9 m. Only the J22 simulation from Group 1a was run for 150 Myr, all other simulations of the SJS system listed into Table 3 were integrated for 200 Myr.

The *Mercury* algorithm was recently modified to model planetary accretion in binary star systems (Chambers et al., 2002), and we used the hybrid symplectic algorithm that is built

in this version to perform the integrations listed in Group 2. In theory, this hybrid algorithm should produce results that are consistent with the hybrid algorithm in the original *Mercury* code. The two simulations in Group 2a, which had identical starting conditions as those in Group 1a, were performed by J.E. Chambers (private communication, 2004), and produced results statistically consistent with Group 1a. The nine simulations in Group 2b (which began with the same initial conditions as the corresponding runs from Group 1b) resulted in fewer planets and more mass loss, on average, than the final systems from Group 1b.

Table 3 gives the average values ( $\bar{x}$ ) for the SJS runs (Group 1 and Group 2), and a statistical comparison (using the Kolmogorov–Smirnov (KS) test) between Group 1b and Group 1c, and between Group 1 and Group 2. The KS value,  $D$ , and the associated probability,  $P$ , show that the planetary statistics of the final planets that form in the J21 set of simulations are consistent with those that formed in the J22 set of runs. Comparing the distributions between Group 1 and Group 2 yield different results. This may be due to the fact that six of the nine runs from Group 2b resulted in two-planet systems, which may be a result of small number statistics. Also note that the simulation which yielded a single planet does not have a finite value for  $S_s$  and  $S_c$ . In this case, the highest value for these statistics is taken when calculating the average,  $D$ , and  $P$ , in order to prevent biased results. We include all of the runs from Group 1 and Group 2 when comparing the final systems that form around close binaries (see Table 2). Finally, Table 3 includes the planetary statistics for 3 simulations that began with the J21 initial disk around the Sun, with neither giant planets nor a stellar companion perturbing the system (Quintana et al., 2002). As expected, the final planetary systems that form in these runs are qualitatively different than when massive companions are included.

## Appendix B. Growth from a disk of planetesimals with forced eccentricities

In our nominal circumbinary disk model, the embryos and planetesimals begin on nearly circular and coplanar orbits about the center of mass of the pair of stars. These initial conditions may not be the most appropriate for simulations in which the binary stars begin with larger stellar separations and higher eccentricities. The least excited state orbiting highly eccentric binary star systems is one in which the bodies in the disk have higher initial eccentricities and aligned arguments of periastron. To examine the magnitude of this effect on the final outcome of the planets that form, we have performed an additional set of simulations of the  $a_B = 0.2$  AU and  $e_B = 0.5$  binary star system (with equal mass stars of  $0.5 M_{\odot}$ ), altering the initial disk conditions according to the following prescription.

We first performed a simulation of the  $a_B = 0.2$  AU and  $e_B = 0.5$  system (omitting the giant planets) with massless test particles, beginning with the coordinates of the planetesimals and planetary embryos in our nominal disk. The particles were followed for 100 years (their eccentricity oscillations ranged

Table 3  
Sun–Jupiter–Saturn simulations

Run	$N_p$	$N_m$	$S_m$	$S_s$	$S_d$	$S_c$	$S_r$	$m_{1*}$ (%)	$m_{1\infty}$ (%)	$E/E_0$	$L/L_0$	$L_Z/L_0$
Group 1a												
J21	4	0	0.335	31.3	0.0061	37.3	0.328	17.14	0.71	1.17	0.91	0.91
J22	4	0	0.326	33.7	0.0105	35.0	0.281	18.57	1.43	1.19	0.91	0.90
Group 1b												
J21_1	3	2	0.532	43.1	0.0048	39.6	0.402	21.43	5.36	1.29	0.87	0.87
J21_2	3	1	0.379	33.3	0.0041	49.3	0.508	18.93	0.00	1.24	0.87	0.87
J21_3	3	1	0.394	36.9	0.0032	34.9	0.518	20.71	0.36	1.16	0.92	0.92
J21_4	3	4	0.400	29.7	0.0132	61.5	0.339	26.79	7.14	1.33	0.84	0.83
J21_5	4	0	0.496	34.0	0.0061	36.3	0.362	20.00	0.00	1.17	0.92	0.91
J21_6	4	2	0.551	35.8	0.0083	34.8	0.296	23.57	0.00	1.23	0.89	0.89
J21_7	2	0	0.571	55.0	0.0118	40.0	0.396	14.64	2.14	1.20	0.89	0.89
J21_8	1	0	1.000	...	0.0686	$\infty$	0.498	34.29	1.79	1.48	0.73	0.72
J21_9	3	0	0.491	52.8	0.0044	22.2	0.411	22.50	1.79	1.26	0.91	0.91
Group 1c												
J22_1	3	3	0.404	36.5	0.0044	34.6	0.414	20.36	0.00	1.20	0.91	0.90
J22_2	3	0	0.518	40.9	0.0117	48.7	0.344	30.36	1.43	1.33	0.84	0.84
J22_3	3	0	0.521	46.0	0.0188	37.5	0.580	22.86	0.36	1.24	0.88	0.87
J22_4	4	0	0.418	33.4	0.0088	36.1	0.255	18.93	0.71	1.18	0.91	0.91
J22_5	3	1	0.392	34.7	0.0069	42.3	0.463	29.64	1.07	1.31	0.86	0.85
J22_6	4	0	0.377	36.0	0.0033	34.1	0.339	18.93	1.43	1.18	0.91	0.91
J22_7	4	0	0.433	37.5	0.0066	33.1	0.311	25.00	0.71	1.25	0.89	0.88
J22_8	3	1	0.381	45.8	0.0260	25.0	0.486	18.93	0.36	1.19	0.92	0.91
J22_9	4	0	0.379	36.8	0.0063	40.2	0.257	25.36	1.43	1.21	0.89	0.89
$\bar{x}$ (Group 1)	3.25	0.75	0.465	39.4	0.0117	39.2	0.389	22.45	1.41	1.24	0.88	0.88
Group 2a												
J21 <sup>a</sup>	4	1	0.488	34.5	0.0122	33.3	0.307	22.50	1.43	1.21	0.90	0.90
J22 <sup>a</sup>	3	1	0.733	42.1	0.0077	81.0	0.412	26.43	0.00	1.26	0.86	0.85
Group 2b												
J21_1 <sup>a</sup>	2	0	0.871	87.0	0.0599	37.4	0.784	29.29	12.50	1.49	0.77	0.76
J21_2 <sup>a</sup>	2	0	0.513	65.9	0.0674	29.0	0.580	29.29	1.07	1.31	0.83	0.82
J21_3 <sup>a</sup>	2	0	0.651	54.2	0.0259	49.0	0.386	25.71	4.64	1.29	0.84	0.84
J21_4 <sup>a</sup>	2	0	0.684	80.8	0.0336	21.4	0.518	32.50	0.71	1.36	0.86	0.85
J21_5 <sup>a</sup>	3	0	0.527	39.8	0.0051	51.2	0.465	32.14	0.71	1.33	0.84	0.84
J21_6 <sup>a</sup>	2	1	0.592	54.6	0.0036	44.0	0.550	26.43	1.79	1.30	0.86	0.86
J21_7 <sup>a</sup>	2	0	0.684	54.3	0.0115	50.0	0.594	25.71	0.71	1.27	0.86	0.86
J21_8 <sup>a</sup>	4	2	0.397	37.2	0.0126	35.9	0.278	16.07	9.29	1.25	0.88	0.88
J21_9 <sup>a</sup>	3	3	0.488	38.3	0.0122	39.2	0.345	26.79	0.71	1.27	0.87	0.87
$\bar{x}$ (Group 2)	2.64	0.73	0.603	53.5	0.0229	42.9	0.474	26.62	3.05	1.30	0.85	0.85
$\bar{x}$ (all)	3.03	0.74	0.514	44.4	0.0157	40.5	0.420	23.93	1.99	1.26	0.87	0.87
Group 1b, Group 1c												
$D$	0.22	0.22	0.44	0.22	0.33	0.33	0.33	0.22	0.44	0.22	0.22	0.22
$P$	0.958	0.958	0.250	0.958	0.603	0.603	0.603	0.958	0.250	0.958	0.958	0.958
Group 1, Group 2												
$D$	0.57	0.25	0.51	0.51	0.44	0.25	0.40	0.62	0.26	0.56	0.57	0.57
$P$	0.012	0.722	0.032	0.032	0.096	0.679	0.147	0.005	0.658	0.014	0.012	0.012
Sun-only												
S_1	4	9	0.462	39.7	0.0136	19.0	0.335	0.000	0.357	1.06	1.00	1.00
S_2	4	8	0.357	38.2	0.0342	16.0	0.359	0.000	1.071	1.05	1.00	0.99
S_3	4	20	0.361	36.7	0.0476	12.8	0.385	0.000	0.000	1.07	1.02	1.00
$\bar{x}$	4	12.3	0.393	38.2	0.0318	15.9	0.360	0.000	0.476	1.06	1.01	1.00
Sun-only, all												
$D$	0.68	0.97	0.52	0.39	0.77	0.75	0.36	0.75	0.49	0.75	0.97	0.97
$P$	0.041	0.001	0.194	0.548	0.012	0.017	0.631	0.017	0.256	0.017	0.001	0.001

<sup>a</sup> Simulations performed using a symplectic hybrid integrator that is incorporated in the close binary code.

from periods of years to decades), and the maximum eccentricity of each test particle,  $e_{\max}$ , was calculated.

We then set up grids with varying values of the eccentricity ( $e/e_{\max}$ ) and argument of periastron ( $\omega$ ) for each of the 154

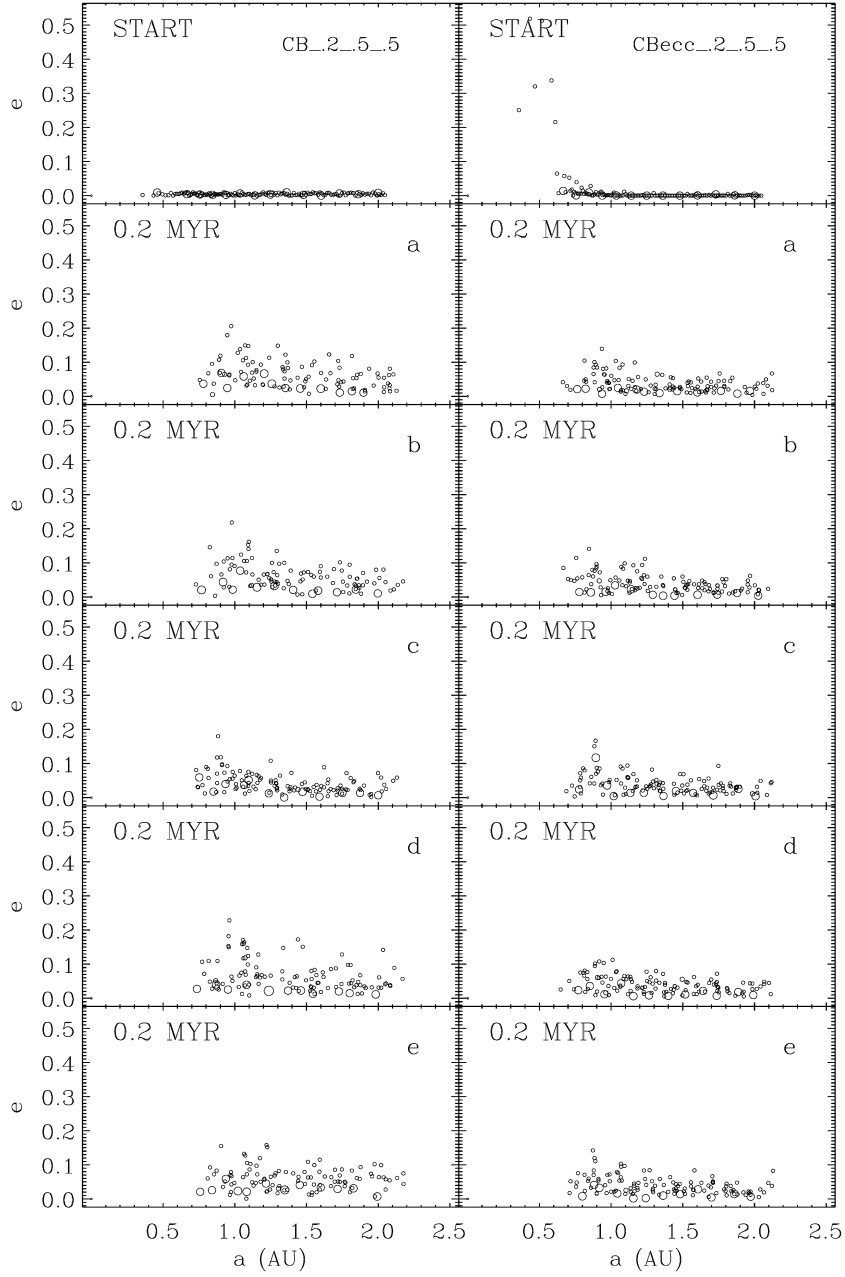


Fig. 9. This figure shows the early evolution of the circumbinary disk around binary stars with  $a_B = 0.2$  AU,  $e_B = 0.5$  and with equal masses of  $M_* = 0.5 M_\odot$ . Jupiter and Saturn are also included. The left column shows our ‘nominal’ disk (that which was used for almost all of the accretion simulations in this article), while the right column shows the disk that began with forced eccentricities. The top row shows each circumbinary disk at the beginning of each simulation, and in subsequent rows the disk at  $t = 200,000$  yr is shown for the five (a–e) simulations. The planetary embryos and planetesimals are represented by circles whose sizes are proportional to the physical sizes of the bodies as in Figs. 1–6. The locations of the circles show the orbital semimajor axes and eccentricities of the represented bodies relative to center of mass of the binary stars.

particles, and ran each system for 100 years in order to find the value of  $(e, \omega)$  that resulted in the smallest range in the magnitude of the eccentricity. We varied  $e$  and  $\omega$  as follows, while keeping the remaining four orbital elements ( $a, i, \Omega$ , and  $M$ , which were randomly selected) constant:

- $0.21 \leq e/e_{\max} \leq 0.7$  (with 0.01 intervals), with 72 values of  $\omega$  (at  $5^\circ$  intervals) examined for each  $e/e_{\max}$ .
- $0.01 \leq e/e_{\max} \leq 0.2$  (with 0.01 intervals), with 36 values of  $\omega$  (at  $10^\circ$  intervals) examined for each  $e/e_{\max}$ .

Within each grid, the particle which had the smallest range of eccentricity ( $e_{\text{sup}} - e_{\text{inf}}$ ) was found, and the initial coordinates of that particle were noted. Excluding the values of semimajor axis at which all bodies were ejected from the system, the preferred value of  $e/e_{\max}$  ranged from 0.01 to 0.66, with an average of 0.096. We then used these new values for the initial orbital elements of the bodies in the circumbinary disk, and performed five simulations with massive planetesimals and embryos, varying the position of one planetesimal in the disk, as done for our other planetary growth simulations.

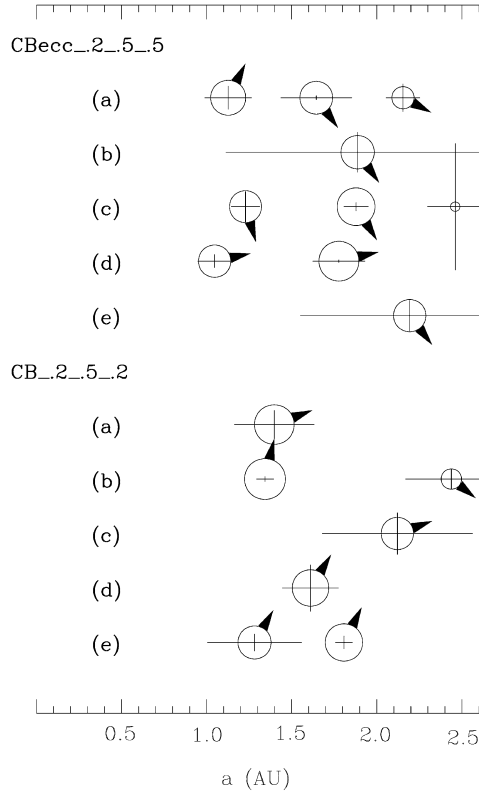


Fig. 10. The final planetary systems for the five simulations of set CBecc\_2\_5\_5 and the five runs of set CB\_2\_5\_5. Note that in run CBecc\_2\_5\_5\_e, an additional planetesimal remains at  $a_p = 18.3$  AU, with  $e_p = 0.26$  and  $i_p = 28^\circ$  relative to the stellar orbit. As in Figs. 7 and 8, symbol sizes are proportional to planet sizes, the centers of the circles are positioned horizontally at the planet's semimajor axis, the horizontal bar represents the extent of the planet's radial excursions, and the vertical bar (which is proportional to the planet's inclination) shows its out of plane motion. All orbital parameters are computed relative to the center of mass of the binary star system. Arrows point in the direction representing the planet's rotational angular momentum. Although a net total of two more major planets were produced in the five CBecc runs, and two planetesimals also survived in these calculations, there is a large variation of planetary systems within each set as a result of chaos. A statistical comparison between the two sets indicates that our choice of initial conditions for our 'nominal' circumbinary disk is sufficient for the accretion simulations presented in this article.

Fig. 9 shows the bodies in the disk at the beginning of the simulation and also at time  $t = 200,000$  years for the CB\_2\_5\_5 (a–e) set (left column) and the CBecc\_2\_5\_5 (a–e) set (right column). Even in this early stage of the simulations, the evolution of the two circumbinary disks are comparable. Fig. 10 presents the final planetary systems for each of these simulations. The planetary statistics (as described in Section 4.1) for the final planetary systems are listed in Table 4 and labeled CBecc\_2\_5\_5 (a–e). Table 4 also re-states the analogous statistics for the five original runs with  $a_B = 0.2$  AU and  $e_B = 0.5$  that we performed, labeled as CB\_2\_5\_5 (a–e). We used a KS test to compare planetary systems resulting from the two sets of simulations, and found that the distributions for each of the statistics listed are statistically consistent. We thus conclude that our choice of initial conditions for our nominal circumbinary disk are sufficient even for the highly eccentric binary star systems examined in this article.

One planetesimal in simulation CBecc\_2\_5\_5\_e ended up stranded in a distant orbit, with periape well beyond the orbits of the giant planets (Fig. 11). This planetesimal was scattered outwards by the giant planets at  $t = 23.6$  yr, and became trapped in a 5:2 resonance with the outer giant planet at  $t = 27.8$  yr. This resonance substantially reduced the planetesimal's eccentricity to  $e = 0.4$ , raising its periape distance to above the apoapse of the orbit of the outermost giant planet (the apoapse of this never exceeded  $Q_{\tilde{\eta}} = 10.84$  AU during the entire integration). The planetesimal broke free of the resonance around  $t = 47.8$  yr, but its periape distance remained high for the remainder of the simulation. It is clearly in a chaotic orbit, capable of returning to the planetary region and being ejected from the system, but this may well not occur for many millions, if not billions, of years. Similar processes may have operated to remove trans-neptunian objects in our Solar System from Neptune's immediate control, and if they happened during the migration epoch of the giant planets, such objects could have been permanently stranded away from the planetary region (Gomes et al., 2005).

Table 4  
Statistics for final planetary systems formed from an eccentric initial disk mass distribution

Run	$t$ (Myr)	$N_p$	$N_m$	$a_p/a_c^*$	$q_p/Q_B$	$S_m$	$S_s$	$S_d$	$S_c$	$S_r$	$m_1$ (%)	$E/E_0$	$L/L_0$	$L_Z/L_{Z_0}$
CBecc_2_5_5_a	200	3	0	1.89	4.22	0.481	33.0	0.0091	95.4	0.211	62.14	0.75	1.10	1.10
CBecc_2_5_5_b	100	1	0	3.17	8.87	1.000	...	0.0975	$\infty$	0.089	84.29	0.55	1.16	1.14
CBecc_2_5_5_c	200	2	2	2.06	4.38	0.610	40.1	0.0048	115.1	0.213	62.50	0.66	1.18	1.17
CBecc_2_5_5_d	200	2	0	1.76	3.82	0.652	48.2	0.0043	83.4	0.120	58.93	0.72	1.13	1.13
CBecc_2_5_5_e	200	1	1	3.68	9.46	0.976	...	0.0564	49.5	0.476	85.36	0.46	1.37	1.35
$\bar{x}$	180	1.8	0.6	2.51	6.15	0.744	43.5	0.0344	91.7	0.222	70.64	0.63	1.19	1.18
CB_2_5_5_a	146	1	0	2.35	5.44	1.000	...	0.0193	$\infty$	0.147	73.58	0.74	1.07	1.07
CB_2_5_5_b	200	2	0	2.25	4.65	0.890	57.2	0.0021	152.4	0.169	67.50	0.73	1.11	1.11
CB_2_5_5_c	154	1	0	3.56	8.54	1.000	...	0.0328	$\infty$	0.378	85.71	0.49	1.31	1.30
CB_2_5_5_d	115	1	0	2.70	5.92	1.000	...	0.0190	$\infty$	0.263	79.29	0.64	1.16	1.15
CB_2_5_5_e	200	2	0	1.78	5.20	0.590	32.4	0.0104	185.7	0.155	62.50	0.67	1.15	1.15
$\bar{x}$	163	1.4	0.0	2.53	5.95	0.896	52.2	0.0167	179.0	0.222	73.72	0.65	1.16	1.16
$D$	...	0.20	0.20	0.40	0.60	0.40	0.60	0.40	0.80	0.40	0.40	0.20	0.20	0.20
$P$	...	1.000	1.000	0.697	0.209	0.697	0.209	0.697	0.036	0.697	0.697	1.000	1.000	1.000

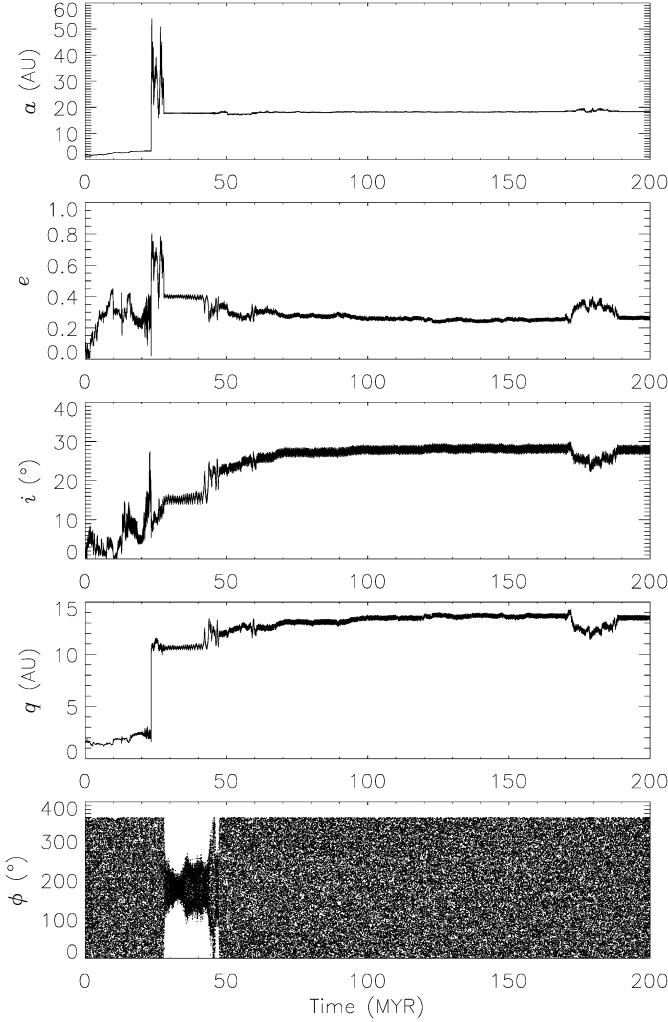


Fig. 11. Evolution of the planetesimal in simulation CBecc\_2\_5\_5\_e that began with  $a = 1.83$  AU,  $e = 0.00015$  and had  $a = 18.3$  AU,  $e = 0.26$  when the simulation was stopped at  $t = 200$  Myr. (a) Semimajor axis. (b) Eccentricity. (c) Inclination. (d) Periape distance. (e) Resonant angle for the 5:2 commensurability with the outer giant planet,  $\phi \equiv 5\lambda_{\text{plmal}} - 2\lambda_{\text{h}} - 3\tilde{\omega}_{\text{plmal}}$  where  $\lambda =$  mean longitude and  $\tilde{\omega} =$  longitude of periastron. Note that once this planetesimal is scattered beyond the giant planets, its eccentricity and inclination are anticorrelated; this suggests that the Kozai mechanism plays an important role in the evolution of the planetesimal’s periape distance.

### Appendix C. Scaling planetary accretion simulations

The ensemble of plausible initial conditions for simulations of planetary growth is immense. Fortunately, one single numerical simulation (or a set thereof) may be valid for a range of stellar and planetary masses, orbital periods, etc. For simulations to correspond exactly, the following must apply:

- (1) The ratios of the masses of all of the bodies must be the same, i.e., there is a uniform factor by which all masses must be multiplied,  $M_*$ .
- (2) The ratios of the distances between objects must be multiplied by an equal amount  $r_*$ , and the physical sizes of the objects, as well as other factors involving removal of objects (inner, outer boundaries in semimajor axis), must be multiplied by this same factor  $r_*$ . Note that, in general, the

densities of objects will change according to the following formula:

$$\rho_* = \frac{M_*}{r_*^3}. \quad (\text{C.1})$$

- (3) Initial (and thus subsequent) velocities must be scaled so that orbital geometries remain the same (“orbital elements”). For this to hold, the ratio of kinetic to potential energy must remain the same, so

$$\frac{Mv^2}{\frac{M^2}{r}} = \text{constant}, \quad (\text{C.2})$$

$$v^2 \propto \frac{M}{r}. \quad (\text{C.3})$$

Therefore,

$$v_* = \left(\frac{M_*}{r_*}\right)^{1/2}. \quad (\text{C.4})$$

- (4) Time must scale in a manner such that the same processes take the same number of orbits, so

$$t_* = \frac{r_*}{v_*} = \left(\frac{r_*^3}{M_*}\right)^{1/2}. \quad (\text{C.5})$$

One example of this scaling is that if the star’s mass is increased, and those of the planetesimals/planetary embryos are increased by the same amount, then the simulations would be applicable either if planetesimal densities increase by this amount or if distances grow by the same factor as the physical radii of the planetesimals. A less trivial example is that a simulation of the growth of rocky planetesimals with  $\rho = 4 \text{ g cm}^{-3}$  at 2 AU corresponds to rock-ice planetesimals with  $\rho = 1.5 \text{ g cm}^{-3}$  at 2.77 AU around the same single star or around another binary with the same masses but with a 38% larger semimajor axis.

Note that we are free to select any positive values for two parameters ( $M_*$  and  $r_*$  in the above discussion), but that these choices specify the values of the other three parameters. Collisional outcomes must also be scaled appropriately, although this is trivially satisfied by the “perfect accretion” assumption used herein. Additionally, any luminosity-related items, temperature related items, radiation forces, etc. (none of which were included in our simulations) must be scaled appropriately.

### References

- Agnor, C.B., Canup, R.M., Levison, H.F., 1999. On the character and consequences of large impacts in the late stage of terrestrial planet formation. *Icarus* 142, 219–237.
- Artymowicz, P., Lubow, S.H., 1994. Dynamics of binary–disk interaction. 1. Resonances and disk gap sizes. *Astrophys. J.* 421, 651–667.
- Chambers, J.E., 1999. A hybrid symplectic integrator that permits close encounters between massive bodies. *Mon. Not. R. Astron. Soc.* 304, 793–799.
- Chambers, J.E., 2001. Making more terrestrial planets. *Icarus* 152, 205–224.
- Chambers, J.E., Quintana, E.V., Duncan, M.J., Lissauer, J.J., 2002. Symplectic integrator algorithms for modeling planetary accretion in binary star systems. *Astron. J.* 123, 2884–2894.

- Correia, A.C.M., Udry, S., Mayor, M., Laskar, J., Naef, D., Pepe, F., Queloz, D., Santos, N.C., 2005. The CORALIE survey for southern extra-solar planets. XIII. A pair of planets around HD 202206 or a circumbinary planet? *Astron. Astrophys.* 440, 751–758.
- Deeg, H.J., Doyle, L.R., Kozhevnikov, V.P., Blue, J.E., Martin, E.L., Schneider, J., 2000. A search for jovian-mass planets around CM Draconis using eclipse minima timing. *Astron. Astrophys.* 358, L5–L8.
- Duquennoy, A., Mayor, M., 1991. Multiplicity among solar-type stars in the solar neighborhood. II. Distribution of the orbital elements in an unbiased sample. *Astron. Astrophys.* 248, 485–524.
- Gomes, R.S., Gallardo, T., Fernandez, J.A., Brunini, A., 2005. On the origin of the high-perihelion scattered disk: The role of the Kozai mechanism and mean motion resonances. *Celest. Mech. Dynam. Astron.* 91, 109–129.
- Holman, M.J., Wiegert, P.A., 1999. Long-term stability of planets in binary systems. *Astron. J.* 117, 621–628.
- Jensen, E.L.N., Koerner, D.W., Mathieu, R.D., 1996. High-resolution imaging of circumstellar gas and dust in UZ Tauri: Comparing binary and single-star disk properties. *Astron. J.* 111, 2431–2438.
- Kortenkamp, S., Wetherill, G.W., 2000. Terrestrial planet and asteroid formation in the presence of giant planets. I. Relative velocities of planetesimals subject to Jupiter and Saturn perturbations. *Icarus* 143, 60–73.
- Lissauer, J.J., 1993. Planet formation. *Annu. Rev. Astron. Astrophys.* 31, 129–174.
- Lissauer, J.J., 2004. Formation of giant planets and brown dwarfs. In: Beaulieu, J.-P., des Etangs, A.L., Terquem, C. (Eds.), *Extrasolar Planets: Today and Tomorrow*. In: ASP Conference Series, vol. 321. ASP, San Francisco, CA, pp. 271–281.
- Lissauer, J.J., Quintana, E.V., Chambers, J.E., Duncan, M.J., Adams, F.C., 2004. Terrestrial planet formation in binary star systems. *Rev. Mex. Astron. Astrofis.* 22, 99–103.
- Lubow, S.H., Artymowicz, P., 2000. Interactions of young binaries with disks. In: Mannings, V., Boss, A.P., Russell, S. (Eds.), *Protostars and Planets IV*. Univ. of Arizona Press, Tucson, pp. 731–755.
- Lyne, A.G., Biggs, J.D., Brinklow, A., McKenna, J., Ashworth, M., 1988. Discovery of a binary millisecond pulsar in the globular cluster M4. *Nature* 332, 45–47.
- Mathieu, R.D., Adams, F.C., Fuller, G.A., Jensen, E.L.N., Koerner, D.W., Sargent, A.I., 1995. Submillimeter continuum observations of the T Tauri spectroscopic binary GW Orionis. *Astron. J.* 109, 2655–2669.
- Mathieu, R.D., Stassun, K., Basri, G., Jensen, E.L.N., Johns-Krull, C.M., Valenti, J.A., Hartmann, L.W., 1997. The classical T Tauri spectroscopic binary DQ Tau. I. Orbital elements and light curves. *Astron. J.* 113, 1841–1854.
- Mathieu, R.D., Ghez, A.M., Jensen, E.L.N., Simon, M., 2000. Young binary stars and associated disks. In: Mannings, V., Boss, A.P., Russell, S. (Eds.), *Protostars and Planets IV*. Univ. of Arizona Press, Tucson, pp. 703–730.
- Moriwaki, K., Nakagawa, Y., 2004. A planetesimal accretion zone in a circumbinary disk. *Astrophys. J.* 609, 1065–1070.
- Muterspaugh, M.W., 2005. *Binary Star Systems and Extrasolar Planets*. Ph.D. thesis, Massachusetts Institute of Technology. 137 pp.
- Pichardo, B., Sparke, L.S., Aguilar, L.A., 2005. Circumstellar and circumbinary discs in eccentric stellar binaries. *Mon. Not. R. Astron. Soc.* 359, 521–530.
- Quintana, E.V., 2003. Terrestrial planet formation around Alpha Centauri B. In: Deming, D., Seager, S. (Eds.), *Scientific Frontiers in Research on Extrasolar Planets*. In: ASP Conference Series, vol. 294. ASP, San Francisco, CA, pp. 319–322.
- Quintana, E.V., 2004. *Planet Formation in Binary Star Systems*. Ph.D. thesis, University of Michigan, Ann Arbor. 249 pp.
- Quintana, E.V., Lissauer, J.J., Chambers, J.E., Duncan, M.J., 2002. Terrestrial planet formation in the  $\alpha$  Centauri system. *Astrophys. J.* 576, 982–996.
- Raghavan, D., Henry, T.J., Mason, B.D., Subasavage, J.P., Jao, W.-C., Beaulieu, T.D., Hambly, N.C., 2006. Two suns in the sky: Stellar multiplicity in exoplanet systems. *Astrophys. J.* 646, 523–542.
- Raymond, S.N., Quinn, T., Lunine, J.I., 2005. The formation and habitability of terrestrial planets in the presence of close-in giant planets. *Icarus* 177, 256–263.
- Safronov, V.S., 1969. *Evolution of the Protoplanetary Cloud and Formation of the Earth and the Planets*. Nauka Press, Moscow.
- Sigurdsson, S., Phinney, E.S., 1993. Binary–single star interactions in globular clusters. *Astrophys. J.* 415, 631–651.
- Sigurdsson, S., Richer, H.B., Hansen, B.M., Stairs, I.H., Thorsett, S.E., 2003. A young white dwarf companion to pulsar B1620-26: Evidence for early planet formation. *Science* 301, 193–196.
- Thebault, P., Marzari, F., Scholl, H., 2006. Relative velocities among accreting planetesimals in binary systems: The circumprimary case. *Icarus* 183, 193–206.
- Udry, S., Mayor, M., Naef, D., Pepe, F., Queloz, D., Santos, N.C., Burnet, M., 2002. The CORALIE survey for southern extra-solar planets. VIII. The very low-mass companions of HD 141937, HD 162020, HD 168443, and HD 202206: Brown dwarfs or “superplanets”? *Astron. Astrophys.* 390, 267–279.
- Weaver, H.A., Stern, S.A., Mutchler, M.J., Steffl, A.J., Buie, M.W., Merline, W.J., Spencer, J.R., Young, E.F., Young, L.A., 2006. Discovery of two new satellites of Pluto. *Nature* 439, 943–945.
- Weidenschilling, S.J., 1977. The distribution of mass in the planetary system and solar nebula. *Astrophys. Space Sci.* 51, 153–158.